REPORT 1263

INVESTIGATION OF THE AERODYNAMIC CHARACTERISTICS OF A MODEL WING-PROPELLER COMBINATION AND OF THE WING AND PROPELLER SEPARATELY AT ANGLES OF ATTACK UP TO 90°†

By Richard E. Kuhn and John W. Draper

SUMMARY

An investigation of the aerodynamic characteristics of a model wing-propeller combination, and of the wing and propeller separately at angles of attack up to 90°, has been conducted in the Langley 300 MPH 7- by 10-foot tunnel. The tests covered thrust coefficients corresponding to free-stream velocities from zero forward speed to the normal range of cruising speeds. The results indicate that increasing the thrust coefficient increases the angle of attack for maximum lift and greatly diminishes the usual reduction in lift above the angle of attack for maximum lift.

Predicted characteristics of an assumed airplane designed for vertical take-off indicate that partial wing stalling would be encountered at certain attitudes but sufficient power was available for flight at any attitude. The effects of slipstream on the variation of lift-curve slope with thrust coefficient for this model could be satisfactorily estimated by means of a modified form of a method formulated by Smelt and Davies. The variation of propeller normal force with angle of attack compared favorably with calculated values. An appreciable direct pitching moment was found to exist on the propeller itself at high angles of attack. This pitching moment was approximately doubled when the propeller was operated in the presence of the wing and corresponded to a downward movement of the effective center of thrust of about 20 percent of the propeller radius.

INTRODUCTION

Numerous schemes have been suggested in an effort to design aircraft that would combine the take-off and landing characteristics of a helicopter with the high-speed potential of a conventional fixed-wing airplane. One of the proposed arrangements involves the use of large-diameter propellers as lifting rotors for the take-off and landing conditions. The cruising attitude is achieved by rotation of the wing-propeller combination through approximately 90°, with the wing providing the lift and the propellers (acting as conventional propellers) providing the thrust required for forward flight.

Results are presented of experimental data obtained with a semispan wing immersed in the slipstream of two large-diameter propellers, and a brief analysis of the application of the data to aircraft combining flight characteristics of the helicopter and conventional airplane. In addition, forces and moments measured on the propeller, when combined with the wing and when separated from the wing, are presented for an angle-of-attack range up to 90°.

SYMBOLS

With a wing operating in the slipstream of a propeller, large forces and moments can be produced even at very small free-stream velocities. In this condition, coefficients based on the free-stream dynamic pressure approach infinity and therefore become meaningless. It appears appropriate, therefore, to base the coefficients on the dynamic pressure in the propeller slipstream. For the present investigation, the coefficients based on this principle are indicated by the use of a double prime and are defined in the list that follows. The positive direction of forces, moments, and angles is indicated in figure 1.

C_L lift coefficient, $\frac{\text{Lift}}{qS/2}$

C_L'' lift coefficient, $\frac{\text{Lift}}{q''S/2}$

C_m'' pitching-moment coefficient, $\frac{\text{Pitching moment}}{q''\bar{c}S/2}$

C_{m_p}'' pitching-moment coefficient of propeller, $\frac{\text{Propeller pitching moment}}{q''S\bar{c}}$

$\Delta C_m''$ increment of total model pitching moment due to propellers, calculated from the measured propeller data,

$$\left(C_{m_p}''+C_{N_p}''\frac{x_{c/4}}{\bar{c}}\right)_{\text{inboard}}+\left(C_{m_p}''+C_{N_p}''\frac{x_{c/4}}{\bar{c}}\right)_{\text{outboard}}$$

C_{N_p}'' normal-force coefficient of propeller, $\frac{\text{Propeller normal force}}{q''S}$

†Supersedes NACA Technical Note 3304 by John W. Draper and Richard E. Kuhn, 1954.

435875—57——17

C_P power coefficient, $\frac{2\pi nQ}{\rho n^3 D^5}$

C_T thrust coefficient, $\frac{T}{\rho n^2 D^4}$

C_X'' longitudinal-force coefficient, $\frac{\text{Longitudinal force}}{q''S/2}$

T_c'' thrust coefficient, $\frac{T}{q''\frac{\pi}{4}D^2}$

b twice span of semispan wing, ft; also, propeller blade chord, ft

c wing chord, ft

$\bar{c}$ mean aerodynamic chord, $\frac{2}{S}\int_0^{b/2} c^2\,dy$, ft

D propeller diameter, ft

d diameter of the fully developed slipstream, ft

d_1 diameter of slipstream at any point, ft

h propeller blade thickness, ft

$K=\frac{x/D}{\sqrt{\frac{1}{4}+\left(\frac{x}{D}\right)^2}}$ (See appendix B.)

N number of propellers

n propeller rotational speed, rps

P propeller shaft power, $\frac{2\pi nQ}{550}$, hp

Q torque, ft-lb

q free-stream dynamic pressure, $\frac{1}{2}\rho V^2$, lb/sq ft

q'' slipstream dynamic pressure, $q+\frac{T}{\frac{\pi}{4}D^2}$, lb/sq ft

R propeller tip radius, ft

r radius to propeller blade element

S twice area of semispan wing, sq ft

T shaft thrust, per propeller, lb

V free-stream velocity, ft/sec

V' velocity at any point in slipstream, ft/sec

ΔV increment of velocity in fully developed slipstream due to thrust, ft/sec

W airplane weight, lb

x longitudinal distance from propeller disk, ft

$x_{\bar{c}/4}$ value of x terminating at $\bar{c}/4$

y spanwise distance from wing root, ft

α angle of attack relative to free-stream velocity, deg

β propeller blade angle, deg

$\beta_{.75R}$ propeller blade angle at 0.75 R, deg

η propeller efficiency, $\frac{TV}{2\pi nQ}$

η'' static thrust efficiency, $\frac{T^{3/2}}{1100P\sqrt{\frac{\rho}{2}\frac{\pi}{4}D^2}}$

Θ angle of inclination of slipstream velocity, deg

λ multiplication factor for increase of lift due to slipstream

ρ mass density of air, slugs/cu ft

ϕ angle of inclination of thrust axis wish respect to free stream, deg

Subscripts:

0 zero angle of attack

p propeller

APPARATUS AND METHODS

MODEL

A semispan wing model of a hypothetical four-engine airplane was used in this investigation. The wing had an aspect ratio of 4.55, a taper ratio of 0.714, and an NACA 0015 airfoil section. A drawing of the model with pertinent dimensions is presented as figure 2 and a photograph of the model mounted for testing is shown as figure 3. The geometric characteristics of the model are given in the following table:

Wing:	
Area (semispan), sq ft	5.125
Span (semispan), ft	3.416
Mean aerodynamic chord, $\bar{c}$, ft	1.514
Root chord, ft	1.75
Tip chord, ft	1.25
Airfoil section	NACA 0015
Aspect ratio	4.55
Taper ratio	0.714
Propellers:	
Diameter, ft	2.0
Disk area, sq ft	3.14
Nacelle diameter, ft	0.33
Airfoil section	Clark Y

The wing was constructed on a steel spar, which served as the support for the two motor nacelles and for the mahogany blocks which form the wing contour. The wing was also equipped with plain flaps that were locked and sealed in the neutral position for this investigation.

The geometric characteristics of the three-blade aluminum-alloy propellers are given in figure 4. The propellers were driven by variable-frequency electric motors rated at 20 horsepower at 18,000 rpm. The motors were operated in parallel from one variable-frequency power supply.

The propeller diameter was too large to permit use of the high design rotational speed of the motors. During the tests, the rotational speed seldom exceeded 6,000 rpm or a propeller tip Mach number of 0.58. The speed of each motor was determined by observing a stroboscopic type of indicator, to which was fed the output frequency of a small alternator connected to the motor shaft. Because both motors were driven from a common power supply, their speeds were usually matched within 10 rpm.

The motors were mounted inside aluminum-alloy nacelles by means of strain-gage beams in order to measure the thrust, torque, normal force, and pitching moment of the propeller and spinner. A photograph of this installation is shown as figure 5.

TESTS

The investigation was conducted in the Langley 300 MPH 7- by 10-foot tunnel. The tests were made at various free-stream dynamic pressures and propeller thrusts so selected as to maintain a constant dynamic pressure of 8 pounds per square foot in the slipstream. Constant thrust on the inboard propeller was maintained by varying the motor speed throughout the angle-of-attack range of −10° to 90°. All data presented were obtained with the outboard propeller rotating in a clockwise direction and the inboard propeller rotating counterclockwise as viewed from behind the propeller. Also, the thrust determined from a given

thrust coefficient at $\alpha=0°$ was held constant throughout the angle-of-attack range. The blade angle on the outboard propeller was adjusted slightly ($\pm 0.1°$ or less) so as to develop the same thrust on this propeller as on the inboard propeller at zero angle of attack. During the tests, the thrust on the two propellers was matched within 0.25 pound for all conditions except for angles of attack above 60° at a thrust coefficient of 0.91. For higher angles of attack, the thrust on the outboard propeller exceeded that desired by as much as 4 pounds. The variations of thrust, dynamic pressure, velocities, and propeller blade angle with thrust coefficient (for each propeller) are tabulated as follows:

T_c''	T, lb	q'', lb/sq ft	$V+\Delta V$, ft/sec	q/q''	$\frac{V}{V+\Delta V}$	$\beta_{.75R}$, deg
0	0	8	82	1.00	1.000	20
.20	5.0	8	82	.80	.894	20
.50	12.5	8	82	.50	.707	8
.71	17.6	8	82	.29	.539	8
.91	22.6	8	82	.09	.300	8
1.00	25.0	8	82	0	0	8

The Reynolds number in the slipstream based on the mean aerodynamic chord of 1.514 feet was 0.8×10^6.

The normal force, pitching moment, thrust, and torque were measured for each propeller at a point of intersection of the shaft center line and the blade axis. The pitching moment, lift, and drag of the complete wing-propeller configuration were measured at the quarter-chord point of the mean aerodynamic chord of the wing. It is emphasized that the wing-propeller data presented herein include the direct propeller forces as well as the forces on the wing.

The propeller-alone tests were made by mounting the propeller-nacelle assembly on a 3-inch-diameter sting, which was supported from the tunnel ceiling by a 3-inch tube located 3 feet behind the propeller disk. The mounting was such that the propeller remained in the center of the tunnel throughout the angle-of-attack range.

The static-thrust calibration of the propeller was made in a large room (18 ft by 42 ft by 10 ft) in order to minimize wall effects.

CORRECTIONS

The data presented have been corrected in the following manner. Approximate corrections for the effect of the tunnel walls on the velocity in the tunnel and in the slipstream were derived and are presented in appendix A. The derivation is based on the simple momentum theory and assumes the slipstream to be parallel to the free stream. For this condition these corrections are small. The applicability of the corrections thus derived for conditions approaching the static thrust and for the high angles of attack may be questionable; however, deviations are assumed to be relatively small and corrections to be fairly accurate for most of the test conditions.

The jet-boundary corrections applied to the angle of attack and longitudinal force were estimated by the method of reference 1. For a given model size, these corrections depend on the circulation about the wing; therefore, the corrections for a particular angle of attack with slipstream have been based on the lift of the wing at that angle of attack without slipstream. The following relationships were used:

$$\alpha=\alpha_{\text{measured}}+0.5\frac{q}{q''}(C_L)_{T_c''=0}$$

$$C_X''=C_X''_{\text{measured}}-0.008\frac{q}{q''}[(C_L)_{T_c''=0}]^2$$

The correction to pitching-moment coefficient was estimated and found to be negligible.

Blockage corrections have not been applied to the data. These corrections were estimated by the method of reference 2 and, with the exception of the wake blockage correction which would become appreciable at the higher angles of attack, the blockage corrections were found to be small. The data can be corrected for the effects of wake blockage at the higher angles of attack by a method derived from reference 2, which can be written in the notation of the present report as follows:

$$q_{\text{corrected}}=q_{\text{measured}}\left[1+\frac{0.036}{(1-T_c'')}\left(C_X''-T_c''\cos\alpha N\frac{\frac{\pi}{4}D^2}{S}\right)\right]$$

REDUCTION OF DATA

The type of flight operation for which the data of this investigation would be useful is one in which the wing-propeller combination is rotated as a unit. An example of this configuration is illustrated in figure 6. For this type of operation, the forward speed may drop to zero so that force and moment coefficients based on the free-stream velocity approach infinity and therefore become meaningless. For the condition in which the wing is largely immersed in the slipstream of a propeller, the forces on the wing would be expected to be largely determined by the dynamic pressure in the slipstream. It appears reasonable, therefore, to base the coefficients on the dynamic pressure in the slipstream.

For this investigation, the dynamic pressure in the slipstream is assumed to be related to the measured thrust by the following momentum-theory equations:

$$T=m_p\Delta V_0=\rho\frac{\pi}{4}D^2\left(V+\frac{\Delta V_0}{2}\right)\Delta V_0$$

where m_p is the mass flow through the propeller and ΔV_0 is the increment of slipstream velocity due to thrust at zero angle of attack. Rearranging terms gives

$$\frac{(\Delta V_0)^2}{2}+V(\Delta V_0)-\frac{T}{\rho\frac{\pi}{4}D^2}=0$$

Solving by the quadratic equation yields

$$\Delta V_0=-V\pm\sqrt{V^2+2\frac{T}{\rho\frac{\pi}{4}D^2}}$$

$$(V+\Delta V_0)^2=V^2+2\frac{T}{\rho\frac{\pi}{4}D^2}$$

This equation may be expressed in terms of the dynamic

pressure as

$$q''_0=q+\frac{T}{\frac{\pi}{4}D^2}$$

The above relationships have been derived for the condition of zero angle of attack of the model. The dynamic pressure in the slipstream would be expected to be a function of angle of attack; however, to include these effects would needlessly complicate the presentation.

For the purpose of presenting coefficients, therefore, the dynamic pressure in the slipstream can be defined as

$$q''=q+\frac{T}{\frac{\pi}{4}D^2} \tag{1}$$

and the thrust coefficient as

$$T_c''=\frac{T}{\frac{\pi}{4}D^2q''}$$

or

$$T_c''\frac{T}{\frac{\pi}{4}D^2q+T} \tag{2}$$

also

$$\frac{q}{q''}=\left(\frac{V}{V+\Delta V_0}\right)^2=1-T_c'' \tag{3}$$

$$\left(\frac{V}{V+\Delta V_0}\right)=\sqrt{1-T_c''} \tag{4}$$

For convenience, some values of the most used terms involving T_c'' have been tabulated in table I.

TABLE I

FUNCTIONS OF T_c''

T_c''	$1-T_c''$	$\sqrt{1-T_c''}$	$\sqrt{1-T_c''}-1$	$1+\sqrt{1-T_c''}$	$1-\sqrt{1-T_c''}$
0	1	1	0	2	0
.1	.90	.949	−.051	1.949	.051
.2	.80	.894	−.106	1.894	.106
.3	.70	.837	−.163	1.837	.163
.4	.60	.774	−.226	1.774	.226
.5	.50	.707	−.293	1.707	.293
.6	.40	.632	−.368	1.632	.368
.7	.30	.548	−.452	1.548	.452
.8	.20	.447	−.553	1.447	.553
.9	.10	.316	−.684	1.316	.684
.92	.08	.283	−.717	1.283	.717
.94	.06	.245	−.755	1.245	.755
.96	.04	.200	−.800	1.200	.800
.98	.02	.141	−.859	1.141	.859
1.0	0	0	−1.000	1.000	1.000

RESULTS AND DISCUSSION

BASIC DATA

Propeller characteristics.—The efficiency curves for the outboard propeller tested alone at various blade angles are presented in figure 7. The maximum efficiency reached (about 0.77) was obtained with a blade angle of 20°, the highest tested.

In order to minimize the time required, the operating conditions were chosen so that only two propeller blade-angle settings were required. A value of $\beta_{.75R}$ of 8° was found to be satisfactory for thrust coefficients of 0.91, 0.71, and 0.50 and $\beta_{.75R}$ of 20° for a thrust coefficient of 0.20.

The choice of blade angle for use at zero forward speed (vertical take-off or landing) cannot be made, however, on the basis of the efficiencies presented in the curves of figure 7. For this purpose, an efficiency factor based on the ability of the propeller to produce static thrust must be used. The static-thrust efficiency can be written in a manner analogous to the figure of merit of rotors:

$$\eta''=\frac{T\frac{\Delta V_0}{2}}{550P}$$

which can be reduced to

$$\eta''=\frac{T^{3/2}}{1100P\sqrt{\frac{\rho}{2}\frac{\pi}{4}D^2}}$$

The maximum static-thrust efficiency of 0.7 shown in figure 7 (diamond symbol) was obtained with a blade angle of 8°. With the propeller disks overlapped, the static-thrust efficiency was reduced to 0.65 as indicated in figure 8. A corresponding reduction in efficiency at forward speeds is indicated in figure 8. This loss in static-thrust efficiency with the propeller disks overlapped does not necessarily mean that overlapping is undesirable, however, because, for an airplane of a given size and with a given number of propellers, overlapping permits the use of larger diameter propellers, which can result in an increase in static thrust for a given horsepower, even though the efficiency is reduced somewhat by overlapping.

The variations of the propeller thrust coefficient C_T and power coefficient C_P with angle of attack are presented in figure 9. It should be remembered when use is made of these data that the thrust was held constant throughout the angle-of-attack range and the rotational speed and power were allowed to decrease with increasing angle of attack. In general, the data for the isolated propeller show somewhat lower values of C_T and C_P than the data for the propeller or propellers operating in the presence of the wing. The biggest differences, however, occur under conditions that are not likely to be of practical interest (high forward speed ($T_c''=0.2$) at high angles of attack). The corresponding variations of $\frac{V\cos\alpha}{nD}$ are presented in figure 10. The power required for a constant thrust condition through the angle-of-attack range is presented in figure 11. In general, the power decreased as the angle of attack increased.

The normal-force and pitching-moment coefficients of the outboard propeller are presented in figure 12. Similar data for the inboard propeller are not presented because of difficulties experienced with the instrumentation for the inboard propeller that resulted in excessive scatter and large shifts in the zero readings. The general trend of the data, however, was similar to that for the outboard propeller. The problems of obtaining reliable data were considerably increased because the strain-gage beams, which measured the normal force and pitching-moment loads, were also required to support the relatively heavy motor and carry the high thrust and torque loads.

Also presented in figure 12 are the theoretical variations of normal force obtained by the method of reference 3. The theoretical variation of propeller normal force with angle of

attack of reference 3 is intended to be applicable only at angles of attack near zero. The additional factors which contribute to the normal force at high angles of attack cannot readily be included in the theoretical treatment. It is interesting to note, however, that, for the configuration of this investigation, calculations of the normal-force coefficient using the q-factor (which accounts for the inflow to the propeller) based on the component of thrust in the free-stream direction rather than in the thrust direction, as assumed in reference 3, show relatively good agreement with the measured data.

The operation of both propellers in the presence of the wing is seen almost to double the pitching moment of the outboard propeller as compared with that of the propeller alone. This magnitude of increase cannot be attributed to an increase in wing-induced upwash at the propeller disk, because such an increase should produce corresponding increases in propeller normal force. It is probable that these increases in pitching moment are due to a change in the velocity through the upper and lower portions of the propeller disk (as referenced to the wing-chord plane). An increase in velocity over the wing (upper part of the propeller disk) would tend to decrease the thrust from the top part of the disk. Conversely, a decrease in velocity through the lower half would increase the thrust of this part of the propeller; thus an increase would occur in the nose-up pitching moment of the propeller with increasing angle of attack.

The propeller pitching moment can be regarded as being due to the fact that thrust of the propeller is applied at some distance from the center of rotation. The effective radial location of the thrust vector is presented in figure 13 and was determined from the pitching-moment data of figure 12 by the following relation

$$\frac{r}{R}=\frac{C_{m_p}''S\bar{c}}{T_c''\,\frac{\pi}{8}D^3}$$

For the most extreme condition, the effective location of the thrust vector is seen to move downward more than 20 percent of the propeller radius. (See sketch, fig. 13).

The significance of these propeller pitching moments can be judged from figure 14, which presents the total contribution of both propellers to the total model pitching moment. Because the data on the inboard propeller was unreliable, the data obtained for the outboard propeller was used for both the inboard and the outboard propellers in the summation represented by $\Delta C_m''$. The calculated variation was obtained by using the calculated values of normal-force coefficients (fig. 12) and letting the pitching-moment coefficient be zero. It can be seen that the usual procedure of basing the propeller contribution only on the propeller normal force accounts for less than half of the total contribution for this configuration at these thrust coefficients. Additional data on the normal force and pitching moments of isolated propellers are presented in references 4 and 5.

The contributions of the spinner (when not rotating) to the propeller normal force and pitching moment are presented in figure 15.

Wing characteristics.—Figure 16 presents the variation with angle of attack and thrust coefficient of the lift coefficient based on the dynamic pressure in the free stream. Figure 17 (a) presents the same data based on the dynamic pressure in the slipstream. The lift variation for a thrust coefficient of 1.0 (dashed line of fig. 17) cannot be presented in figure 16 because, if the free-stream dynamic pressure were used to obtain the coefficient, the lift coefficient at all angles of attack would be infinite. The disadvantage of basing the coefficients on the free-stream dynamic pressure is thus readily apparent.

Increasing the thrust coefficient, with either one propeller (fig. 18) or two propellers (fig. 17), results in an increase in the angle of attack at which maximum lift is reached and a more gradual variation of the lift with angle of attack above maximum lift. It should be remembered that these results are for constant thrust throughout the angle-of-attack range. If the power were held constant as the angle of attack was increased, the thrust would increase with angle of attack and an even more gradual variation of lift above maximum lift would be indicated.

The data at $T_c''=0$ (figs. 17 and 18) were obtained with the propellers removed. Data are compared in figure 19 for conditions of propeller removed, of zero thrust with the propeller on, and of propeller windmilling. Removing the propeller results in a small reduction in lift in the region of maximum lift. As would be expected from the propeller data discussed previously, removing the propellers appreciably decreases the unstable variation of pitching moment with angle of attack at the low angles of attack. These effects should be kept in mind when the propeller-off pitching-moment data of figures 17 and 18 are used.

The data of figure 20 indicate, as might be expected, that the nacelles disturb the flow over the wing so that the wing with nacelles stalls at a lower angle of attack and lower lift coefficient than the wing alone. As would be expected, the nacelles also cause a marked decrease in the static longitudinal stability $\left(\text{increase in } \frac{\partial C_m''}{\partial \alpha}\right)$ below the stall.

The destabilizing effects of the propellers and nacelles at zero angle of attack are summarized in figure 21. These data show that, near zero angle of attack, there is only a small variation of stability, as indicated by the curve of $\frac{\partial C_m''}{\partial C_L''}$ against thrust coefficient.

Estimation of the lift-curve slope.—Reference 6 presents relationships for estimating the increase of lift due to a slipstream flowing over the wing. Rearranging the relationship to provide an expression for the lift-curve slope of the wing with slipstream and using the notation of the present report gives the following equation:

$$\frac{\partial C_L''}{\partial \alpha}=\left(\frac{\partial C_L}{\partial \alpha}\right)_{T_c''=0}(1-T_c'')\left\{1+\frac{d_1c}{S}\left(\frac{V'}{V}-1\right)\left[\lambda-0.6\left(\frac{2\pi}{57.3}\right)\left(\frac{1}{(\partial C_L/\partial\alpha)_{T_c''=0}}\right)\left(\frac{\Theta}{\alpha}\right)\right]\right\} \quad (5)$$

For the present configuration, λ can be taken as 1.0 (ref. 6),

$\left(\frac{V'}{V}-1\right)$ is obtained from equation (B5) of appendix B, $\frac{\Theta}{\alpha}=\frac{\Theta}{\phi}$ is obtained from equation (B7) of appendix B, and

$$0.6\left(\frac{2\pi}{57.3}\right)\left(\frac{1}{(\partial C_L/\partial\alpha)_{T_c''=0}}\right)\approx 1$$

The lift-curve slope can be expressed as

$$\frac{\partial C_L''}{\partial\alpha}=\left(\frac{\partial C_L}{\partial\alpha}\right)_{T_c''=0}(1-T_c'')\left[1+\frac{d_1c}{S}\left(\frac{1-\sqrt{1-T_c''}}{1+\sqrt{1-T_c''}}\right)(1+K)\right] \tag{6}$$

where d_1 can be obtained from equation (B4) of appendix B. Calculation of the lift-curve slope by this equation underestimates the measured lift-curve slope (fig. 22).

If it is assumed that the inclination of the slipstream is zero $\left(\frac{\Theta}{\alpha}=0\right)$, equation (5) reduces to

$$\frac{\partial C_L''}{\partial\alpha}=\left(\frac{\partial C_L}{\partial\alpha}\right)_{T_c''=0}(1-T_c'')\left[1+\frac{d_1c}{S}\left(\frac{1-\sqrt{1-T_c''}}{2\sqrt{1-T_c''}}\right)(1+K)\right] \tag{7}$$

and much better agreement with the experimental data is obtained (fig. 22). This equation, in effect, is based on the assumption that the circulation around the wing is unchanged by the presence of the slipstream and the increase in lift is directly proportional to the increase in velocity across the circulation.

If it is further assumed that the wing is far enough behind the propeller so that the full slipstream velocity is developed ($K=1$) and that the wing is fully immersed in the slipstream $\left(\frac{d_1c}{S}=1\right)$, the equation reduces to the simple form

$$\frac{\partial C_L''}{\partial\alpha}=\left(\frac{\partial C_L}{\partial\alpha}\right)_{T_c''=0}\sqrt{1-T_c''} \tag{8}$$

According to equation 7, the fact that the lift-curve slope obtained for the configuration with two propellers is higher than that obtained for the configuration with one propeller is primarily due to the greater percentage of wing area that is immersed in the slipstream.

PERFORMANCE ESTIMATES

The procedure outlined in appendix C was used to estimate the performance of a hypothetical four-propeller airplane as it traversed the regime of flight represented in figure 6. The hypothetical airplane was assumed to have linear dimensions 6 times those of the model. Calculations were made for standard sea-level conditions, and the fuselage and other parts of the airplane not represented by the model were assumed to have a drag coefficient of 0.01.

The variation of the thrust coefficient required and the forward velocity reached in constant-altitude transition, as the wing attitude is lowered from 90° for take-off to conventional flight attitude, is shown in figure 23. The corresponding variation of thrust power required with forward velocity for an assumed wing loading of 40 pounds per square foot is shown in figure 24. The thrust power required is seen to decrease quite rapidly in the low speed range. The minimum thrust power required occurs in the normal flight range at a speed of 160 mph and a wing attitude of 8.5°. It will be noted that (with the assumption that $\eta=0.75$ at high speed and $\eta''=0.65$ for static-thrust take-off), if this airplane were designed for a high speed of the order of 350 to 400 mph, sufficient power would be available for vertical take-off with the 12-foot-diameter propellers represented by the ones used on this model.

The untrimmed pitching moment and corresponding effective aerodynamic-center location, as indicated by $\frac{\partial C_m''}{\partial C_L''}$ for the conditions of this analysis, are indicated in figure 25. No allowance for the effects of trimming these moments was made in this analysis. These data are based on the assumption that the center of gravity of the airplane is located at the pivot axis of the wing and that this axis is located at the quarter-chord point of the mean aerodynamic chord. Figure 25 (c) indicates that a more forward location of the pivot axis would be desirable in reducing the out-of-trim moments. Figure 25 (a) indicates that, for the present configuration, a full-span, 30-percent-chord trailing-edge flap (ref. 7) would be ineffective in balancing the airplane. The complete loss in effectiveness in the angle-of-attack range from 56° to 77° indicates that the wing is partially stalled in this angle-of-attack range. Results of an unpublished investigation indicate that, with the propellers placed much closer to the wing, this reduction in control effectiveness may be greatly reduced.

CONCLUSIONS

An investigation of the aerodynamic characteristics of a wing-propeller combination and of the wing and propeller separately at angles of attack up to 90° indicates the following conclusions:

1. Increasing the thrust coefficient increased the angle of attack for maximum lift coefficient and greatly diminished the reduction of lift coefficient above the angle of attack for maximum lift. Analysis of the operation of a hypothetical airplane designed for vertical take-off indicated that partial wing stalling probably would be encountered in certain flight attitudes but sufficient power would be available for flights at any attitude.

2. The effects of slipstream on the variation of the lift-curve slope with thrust coefficient would be satisfactorily estimated for this model by means of a modified form of a method formulated by Smelt and Davies.

3. The variation of propeller normal force with angle of attack compared favorably with calculated values. There was also an appreciable direct pitching moment on the propeller itself. This pitching moment was approximately doubled when the propeller was operated in the presence of the wing and corresponded to a downward movement of the effective center of thrust of approximately 20 percent of the propeller radius.

4. Calculations for a hypothetical airplane, with a wing loading of 40 pounds per square foot and the relationship of the total propeller disk area to wing area represented by this model, indicate that airplanes designed for a high speed range of 350 to 400 mph will have sufficient power available for vertical take-off.

LANGLEY AERONAUTICAL LABORATORY,
NATIONAL ADVISORY COMMITTEE FOR AERONAUTICS,
LANGLEY FIELD, VA., *August 13, 1954.*

APPENDIX A

TUNNEL-WALL CORRECTIONS

In order to correct the wind-tunnel data for tunnel-wall effects the following relations for velocities were obtained in a manner similar to that presented in reference 8. The symbols that are used in this appendix and which have not been defined previously are defined as follows:

A	propeller disk area, $\frac{\pi}{4}D^2$, sq ft
C	tunnel cross-sectional area, sq ft
s	slipstream cross-sectional area, sq ft
p	static pressure lb/sq ft
V	local velocity, ft/sec
K_1	ratio of free-stream velocity to slipstream velocity, $\frac{V_0}{V_3}$

Subscripts:

0	far ahead of propeller disk
1	in tunnel at propeller disk but outside of slipstream
2	in tunnel far behind propeller disk but outside of slipstream
3	in slipstream far behind propeller disk
4	immediately behind propeller disk
5	immediately ahead of propeller disk
x	at any station

The following sketch shows the relative location of the stations at which the velocities, pressures, and areas used in the following equations were obtained:

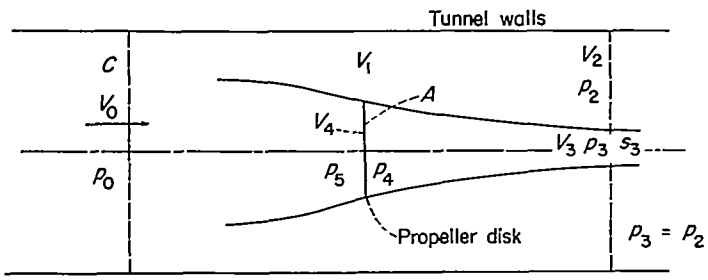

The relationships of pressure and velocity as determined by Bernoulli's equation for a station in front of the propeller, behind the propeller disk, and outside the slipstream tube are as follows:.

Ahead of propeller:

$$p_0+\frac{1}{2}\rho V_0^2=p_5+\frac{1}{2}\rho V_4^2 \tag{A1}$$

Behind propeller:

$$p_4+\frac{1}{2}\rho V_4^2=p_3+\frac{1}{2}\rho V_3^2 \tag{A2}$$

Outside of propeller:

$$p_0+\frac{1}{2}\rho V_0^2=p_2+\frac{1}{2}\rho V_2^2 \tag{A3}$$

Also, assume

$$p_3=p_2 \tag{A4}$$

Solving for $\frac{1}{2}\rho V_4^2$ in equations (A1) and (A2) and equating gives

$$p_0-p_5+\frac{1}{2}\rho V_0^2=p_3-p_4+\frac{1}{2}\rho V_3^2 \tag{A5}$$

Also,

$$p_4-p_5=\Delta p=\frac{T}{A} \tag{A6}$$

Solving for p_4-p_5 in equation (A5) and substitution in equation (A6) gives

$$\frac{T}{A}=p_3-p_0+\frac{1}{2}\rho V_3^2-\frac{1}{2}\rho V_0^2 \tag{A7}$$

and, from equations (A3) and (A4),

$$p_3-p_0-\frac{1}{2}\rho V_0^2=-\frac{1}{2}\rho V_2^2 \tag{A8}$$

Then, from equations (A7) and (A8),

$$\frac{T}{A}=\frac{\rho}{2}(V_3^2-V_2^2) \tag{A9}$$

By definition,

$$T_c''=\frac{T}{\frac{\rho}{2}AV_3^2} \tag{A10}$$

and from equation (A9)

$$T_c''=1-\left(\frac{V_2}{V_3}\right)^2 \tag{A11}$$

From the continuity that $AV=A_xV_x$, the cross-sectional area of the slipstream can be obtained; thus

$$V_0C=V_1(C-A)+V_4A=V_2(C-s)+V_3s$$

$$V_0C=V_2C-V_2s+V_3s$$

$$s=C\frac{(V_0-V_2)}{(V_3-V_2)} \tag{A12}$$

Solution for the thrust from the equations for axial momentum is obtained by the use of the following equations:

$$T=s\rho V_3(V_3-V_0)-(C-s)\rho V_2(V_0-V_2)+C(p_2-p_0) \tag{A13}$$

Substituting for (p_2-p_0) from equation (A3) gives

$$T=s\rho V_3(V_3-V_0)-(C-s)(\rho V_2)(V_0-V_2)+C\frac{\rho}{2}(V_0^2-V_2^2) \tag{A14}$$

Substituting for s from equation (A12) into equation (A14)

and solving for V_0 gives

$$V_0=(V_3+V_2)\pm\sqrt{V_3^2-\frac{2T}{C\rho}} \tag{A15}$$

Substitute $T=\frac{\rho}{2}A\,(V_3^2-V_2^2)$ from equation (A9) into equation (A15) to obtain

$$V_0=(V_3+V_2)\pm\sqrt{V_3^2-\frac{A}{C}(V_3^2-V_2^2)} \tag{A16}$$

But, from equation (A11), $V_3^2=\frac{V_2^2}{1-T_c''}$, so that substituting into equation (A16) and using the minus sign gives

$$V_0=V_2\left(\frac{1+\sqrt{1-T_c''}-\sqrt{1-\frac{A}{C}T_c''}}{\sqrt{1-T_c''}}\right) \tag{A17}$$

Also,

$$V_0=V_3\left(1+\sqrt{1-T_c''}-\sqrt{1-\frac{A}{C}T_c''}\right) \tag{A18}$$

A simplification can be effected by assuming that

$$V_0=V_3K_1$$

Then,

$$V_0=V_2\frac{K_1}{\sqrt{1-T_c''}}$$

where

$$K_1=1+\sqrt{1-T_c''}-\sqrt{1-\frac{A}{C}T_c''} \tag{A19}$$

The equations for slipstream area and velocities are then as follows:

$$s=C\left(\frac{1-\frac{\sqrt{1-T_c''}}{K_1}}{\frac{1}{K_1}-\frac{\sqrt{1-T_c''}}{K_1}}\right)=C\left(\frac{K_1-\sqrt{1-T_c''}}{1-\sqrt{1-T_c''}}\right)$$

$$s=C\frac{1-\sqrt{1-\frac{A}{C}T_c''}}{1-\sqrt{1-T_c''}} \tag{A20}$$

From equation (A17)

$$V_2=(\sqrt{1-T_c''})\frac{V_0}{K_1} \tag{A21}$$

From equation (A18)

$$V_3=\frac{V_0}{K_1} \tag{A22}$$

From continuity, $V_4A=V_3s$ so that, with equations (A20) and (A22),

$$V_4=\left(\frac{V_0}{K_1}\right)\left(\frac{C}{A}\right)\left(\frac{1-\sqrt{1-\frac{A}{C}T_c''}}{1-\sqrt{1-T_c''}}\right) \tag{A23}$$

Since, from continuity,

$$V_0C=V_4A+V_1(C-A)$$

equation (A23) can be used to obtain

$$V_1=\frac{V_0C\left[1-\frac{1}{K_1}\left(\frac{1-\sqrt{1-\frac{A}{C}T_c''}}{1-\sqrt{1-T_c''}}\right)\right]}{C-A} \tag{A24}$$

APPENDIX B

SLIPSTREAM CHARACTERISTICS

The following relationships concerning the character of the slipstream are helpful in analyzing the effects of slipstream on the aerodynamic characteristics of wings.

Diameter of the slipstream at any T_c'' and any distance behind the propeller.—Reference 6 gives a relation for the velocity at any point in the slipstream as

$$V'=V+\frac{\Delta V}{2}\left(1+\frac{x/D}{\sqrt{\frac{1}{4}+\left(\frac{x}{D}\right)^2}}\right)=V+\frac{\Delta V}{2}(1+K) \tag{B1}$$

where V' is the velocity at distance x from the propeller disk. If the mass flow in the slipstream is assumed to be constant, then,

$$\rho\frac{\pi}{4}D^2\left(V+\frac{\Delta V}{2}\right)=\rho\frac{\pi}{4}d_1^2V'$$

$$d_1^2=D^2\frac{\left(V+\frac{\Delta V}{2}\right)}{V'}=D^2\frac{1+\frac{\Delta V}{2V}}{1+\frac{\Delta V}{2V}(1+K)} \tag{B2}$$

where d_1 is the diameter of the slipstream at distance x from the propeller disk and

$$K=\left(\frac{x/D}{\sqrt{\frac{1}{4}+\left(\frac{x}{D}\right)^2}}\right)$$

From equation (4) of the main body of this report,

$$\frac{\Delta V}{2V}=\frac{1-\sqrt{1-T_c''}}{2\sqrt{1-T_c''}} \tag{B3}$$

Equation (B3) can be substituted into equation (B2) and the result simplified to obtain

$$d_1^2=D^2\frac{1+\sqrt{1-T_c''}}{2+(\sqrt{1-T_c''}-1)(1-K)} \tag{B4}$$

Also, from equations (B1) and (B3),

$$\frac{V'}{V}-1=\frac{\Delta V}{2V}(1+K)=\frac{1-\sqrt{1-T_c''}}{2\sqrt{1-T_c''}}(1+K) \tag{B5}$$

Inclination of the slipstream.—From reference 6 the following relationship for the inclination of the slipstream to the

free stream at small angles of attack can be obtained.

$$\theta=\frac{\phi\frac{\Delta V}{2V}}{1+\frac{\Delta V}{2V}} \tag{B6}$$

From equations (B3) and (B6)

$$\frac{\theta}{\phi}=\frac{1-\sqrt{1-T_c''}}{1+\sqrt{1-T_c''}} \tag{B7}$$

where ϕ is the inclination of the thrust axis and θ is the inclination of the slipstream at the propeller disk.

APPENDIX C

PERFORMANCE CALCULATIONS

Calculation of the performance by use of coefficients based on the dynamic pressure in the slipstream required some modification of conventional procedures. The thrust coefficient required for steady level flight at a particular attitude can be obtained by cross plotting the longitudinal force to determine the thrust coefficient for zero longitudinal force. Similar cross plots of lift coefficient can be used to determine the lift coefficient available at this thrust coefficient. The forward speed corresponding to this thrust coefficient and lift coefficient is calculated by the following equation

$$V_{mph}=\frac{60}{88}\sqrt{\left(\frac{W/S}{C_L''}\right)\frac{(1-T_c'')}{\rho/2}} \tag{C1}$$

The total thrust at this thrust coefficient is given by

$$NT=T_c''\left(\frac{W/S}{C_L''}\right)\frac{\pi}{4}D^2N \tag{C2}$$

The thrust horsepower required for steady level flight can be calculated from momentum relations from the following basic equation:

$$\text{thp}_{\text{required}}=\frac{NTV\cos\alpha}{550}+\frac{NT\frac{\Delta V}{2}}{550} \tag{C3}$$

where the first term represents the power required to overcome the drag and the second term represents the power in the slipstream. In the speed range of conventional airplanes the second term is negligible and cos α is approximately unity. The power required equation then reduces to the conventional

$$\text{thp}_{\text{required}}=\frac{NTV}{550}$$

The increment of velocity in each slipstream due to thrust ΔV can be obtained from the momentum relation

$$T=m_p\Delta V=\rho\frac{\pi}{4}D^2\left(V\cos\alpha+\frac{\Delta V}{2}\right)\Delta V$$

where m_p is the mass flow through the propeller and

$$\Delta V=\sqrt{V^2\cos^2\alpha+\frac{T}{\frac{\rho}{2}\frac{\pi}{4}D^2}}-V\cos\alpha \tag{C4}$$

For vertical take-off and landing, V is zero and the power required (eq. (C3)) reduces to

$$\text{thp}_{\text{required}}=\frac{NT\frac{\Delta V}{2}}{550}=\frac{N(T)^{3/2}}{1100\frac{D}{2}\sqrt{(\rho/2)\pi}} \tag{C5}$$

For intermediate flight conditions at low speed, the power required (eq. (C3)) can be expressed as

$$\text{thp}_{\text{required}}=\frac{NTV}{550}\left(\frac{\cos\alpha+\sqrt{\cos^2\alpha+\frac{T}{\frac{1}{2}\rho V^2\frac{\pi}{4}D^2}}}{2}\right) \tag{C6}$$

which can be expressed in terms of the thrust coefficient as

$$\text{thp}_{\text{required}}=\frac{NTV}{550}\left(\frac{\cos\alpha+\sqrt{\cos^2\alpha+\frac{T_c''}{1-T_c''}}}{2}\right) \tag{C7}$$

REFERENCES

1. Gillis, Clarence L., Polhamus, Edward C., and Gray, Joseph L., Jr.: Charts for Determining Jet-Boundary Corrections for Complete Models in 7- by 10-Foot Closed Rectangular Wind Tunnels. NACA WR L-123, 1945. (Formerly NACA ARR L5G31.)
2. Herriot, John G.: Blockage Corrections for Three-Dimensional-Flow Closed-Throat Wind Tunnels, With Consideration of the Effect of Compressibility. NACA Rep. 995, 1950. (Supersedes NACA RM A7B28.)
3. Ribner, Herbert S.: Notes on the Propeller and Slipstream in Relation to Stability. NACA WR L-25, 1944. (Formerly NACA ARR L4I12a.)
4. Lesley, E. P., Worley, George F., and Moy, Stanley: Air Propellers in Yaw. NACA Rep. 597, 1937.
5. McLemore, H. Clyde, and Cannon, Michael D.: Aerodynamic Investigation of a Four-Blade Propeller Operating Through an Angle-of-Attack Range From 0° to 180°. NACA TN 3228, 1954.
6. Smelt, R., and Davies, H.: Estimation of Increase in Lift Due to Slipstream. R. & M. No. 1788, British A.R.C., 1937.
7. Kuhn, Richard E., and Draper, John W.: An Investigation of a Wing-Propeller Configuration Employing Large-Chord Plain Flaps and Large-Diameter Propellers for Low-Speed Flight and Vertical Take-Off. NACA TN 3307, 1954.
8. Glauert, H.: The Elements of Aerofoil and Airscrew Theory. Sec. ed., Cambridge Univ. Press, 1947. (Reprinted 1948.)

435875—57——18

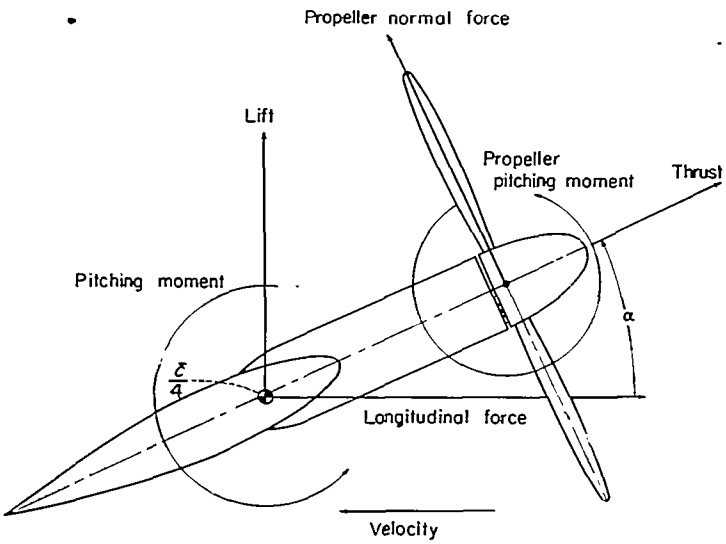

FIGURE 1.—System of axes showing positive direction of forces, moments, and angles.

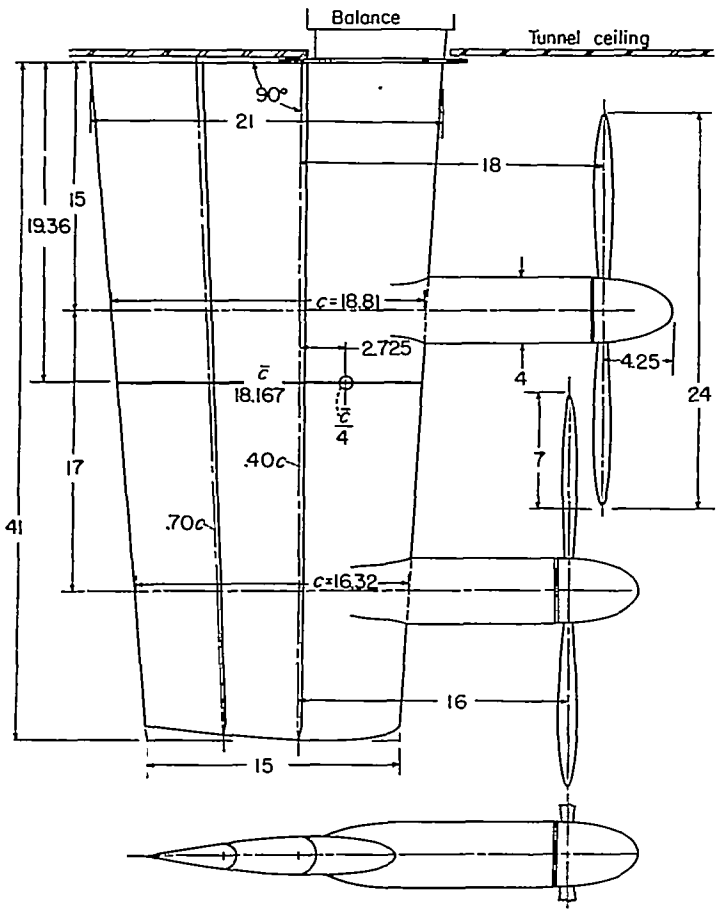

FIGURE 2.—Plan and cross-sectional views of model. (All dimensions are in inches.)

FIGURE 3.—Model installed in the test section of the Langley 300 MPH 7- by 10-foot tunnel.

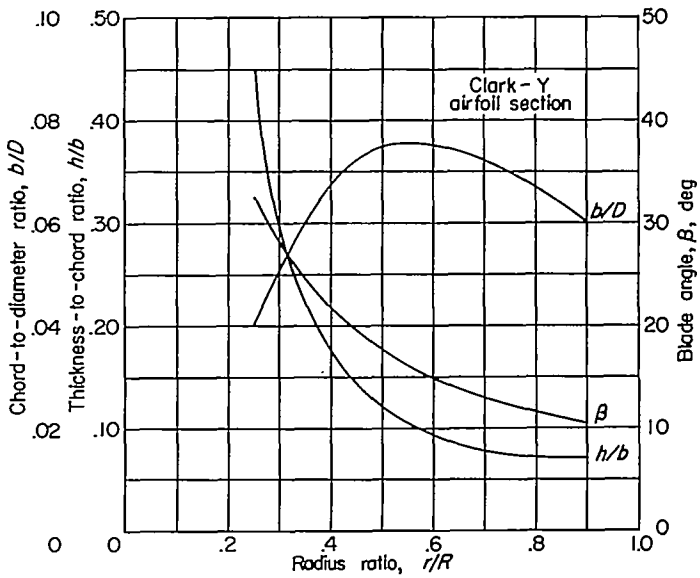

FIGURE 4.—Propeller-blade geometric characteristics.

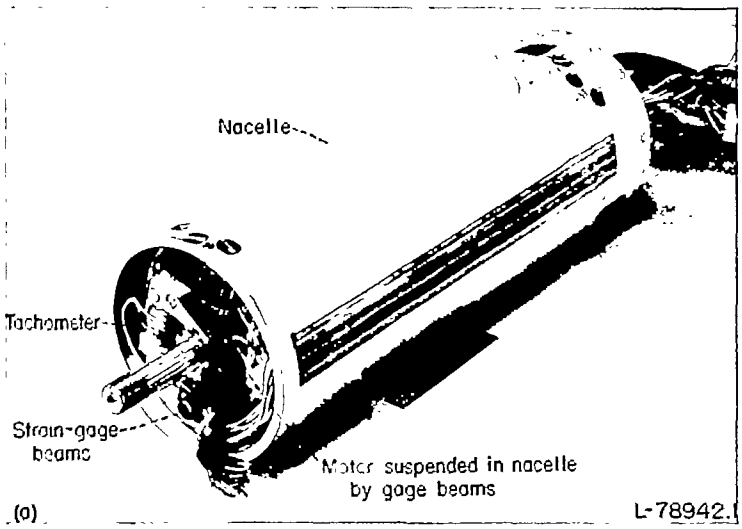

(a) Complete motor balance.

FIGURE 5.—Motor-balance installation used for tests.

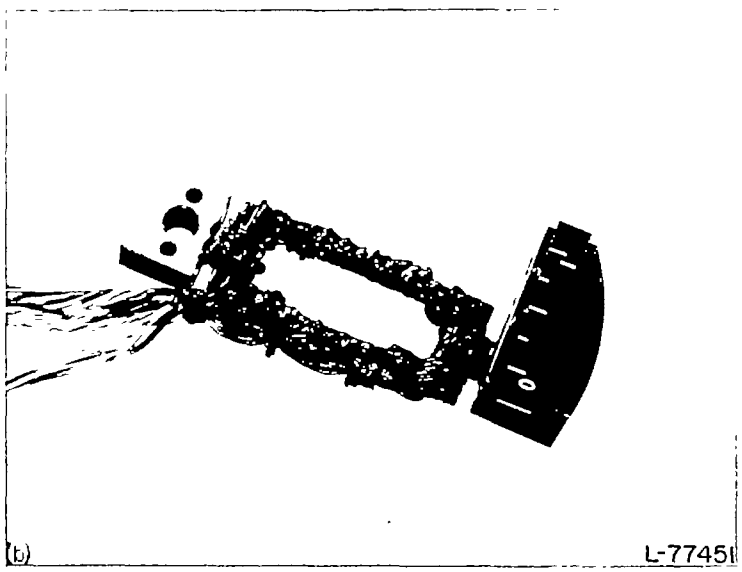

(b) Strain-gage beam used in measuring forces on propeller.

FIGURE 5.—Concluded.

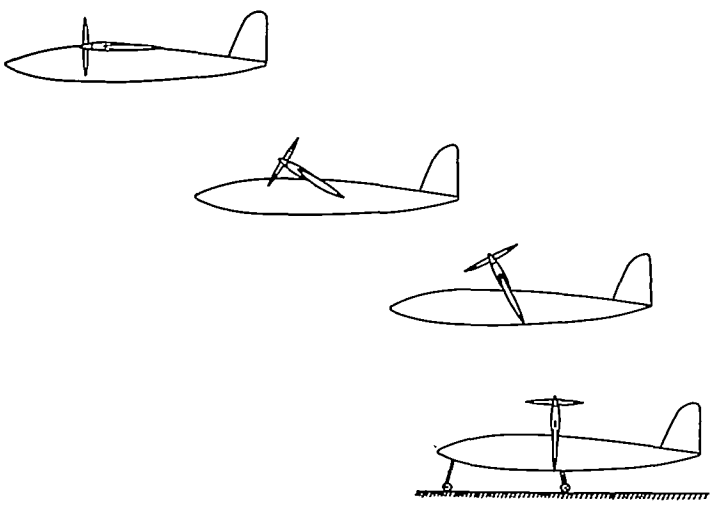

FIGURE 6.—Illustration of a method for vertical take-off and translation to horizontal flight for which data are applicable.

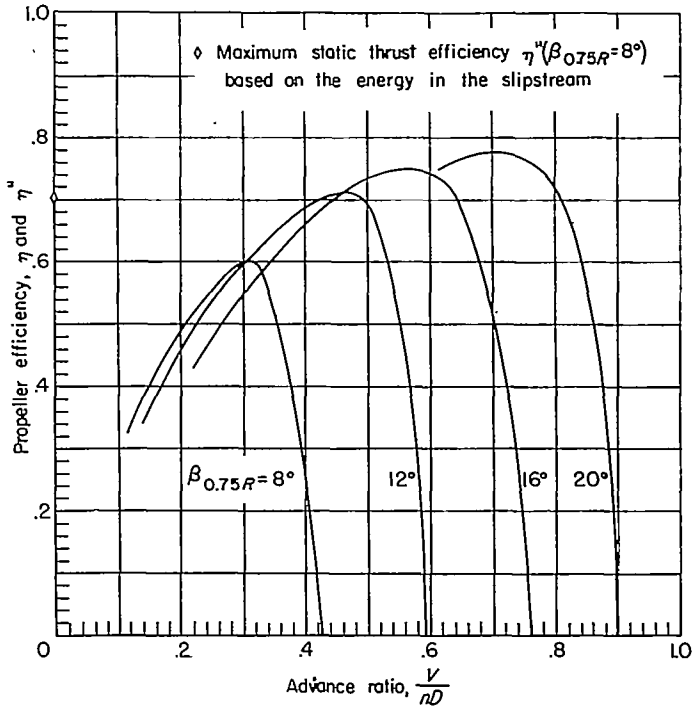

FIGURE 7.—Efficiency of the isolated propeller.

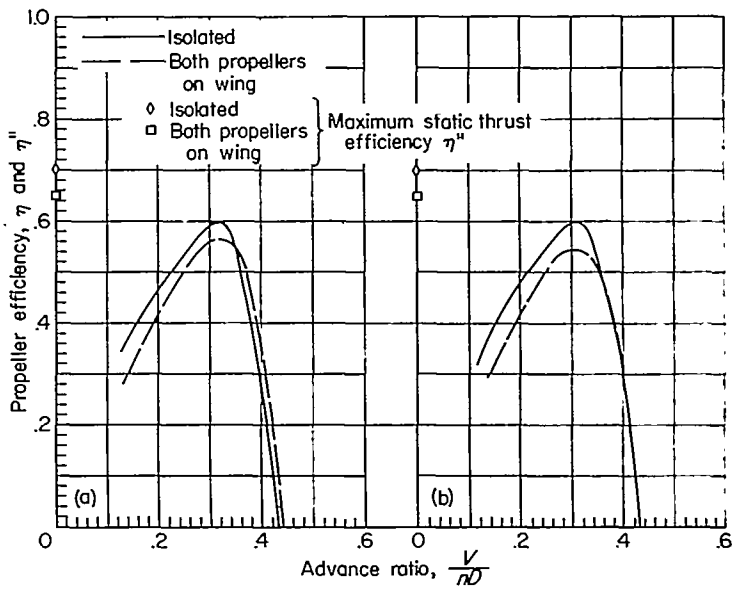

(a) Inboard propeller. (b) Outboard propeller.

FIGURE 8.—Comparison of efficiency of the isolated propeller with that of two overlapping propellers mounted on the wing as shown in figure 2. $\beta_{0.75R}=8°$.

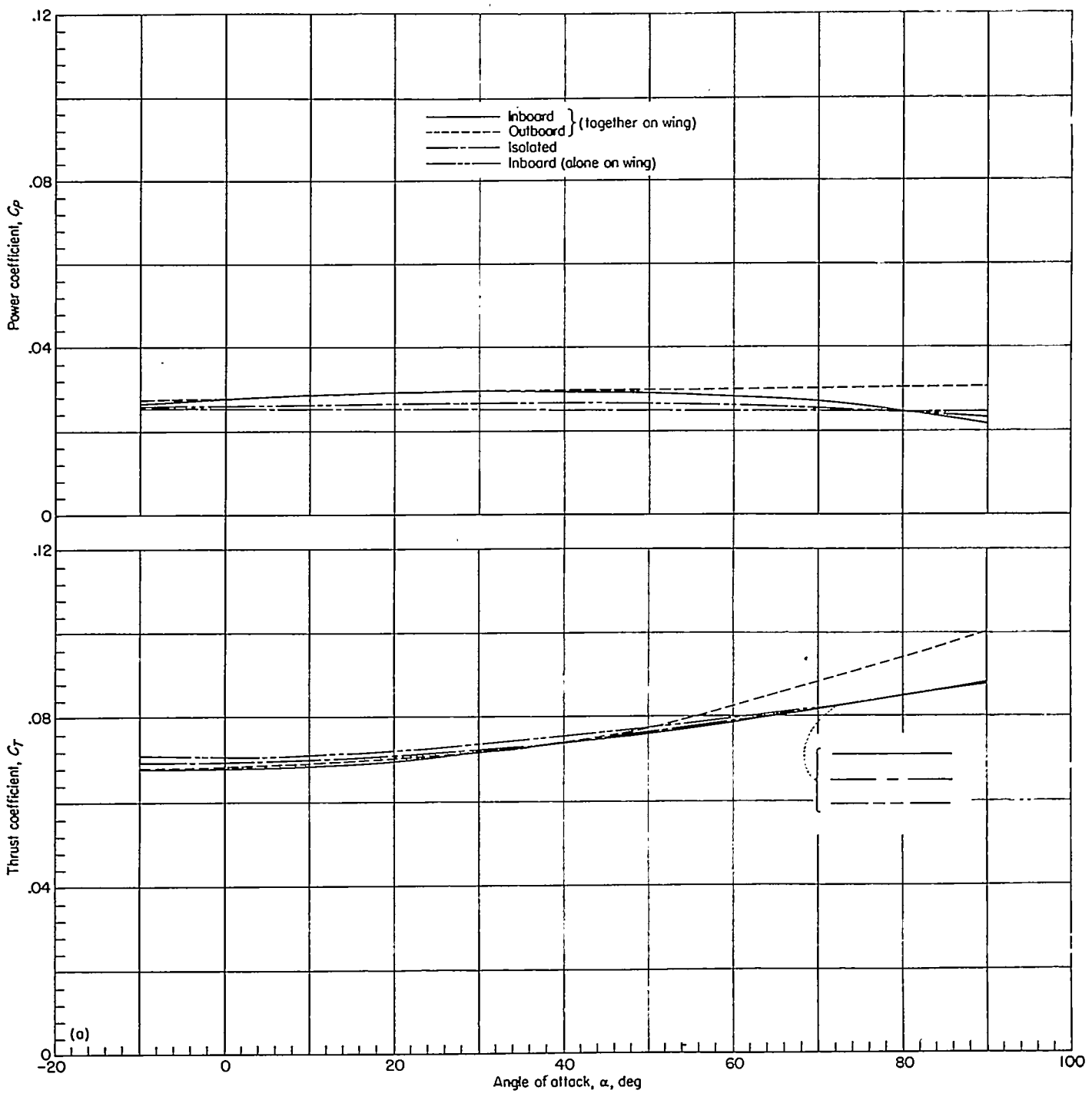

(a) $T_c''=0.91$; $\beta_{0.75R}=8°$.

FIGURE 9.—Propeller characteristics through angle-of-attack range with constant shaft thrust.

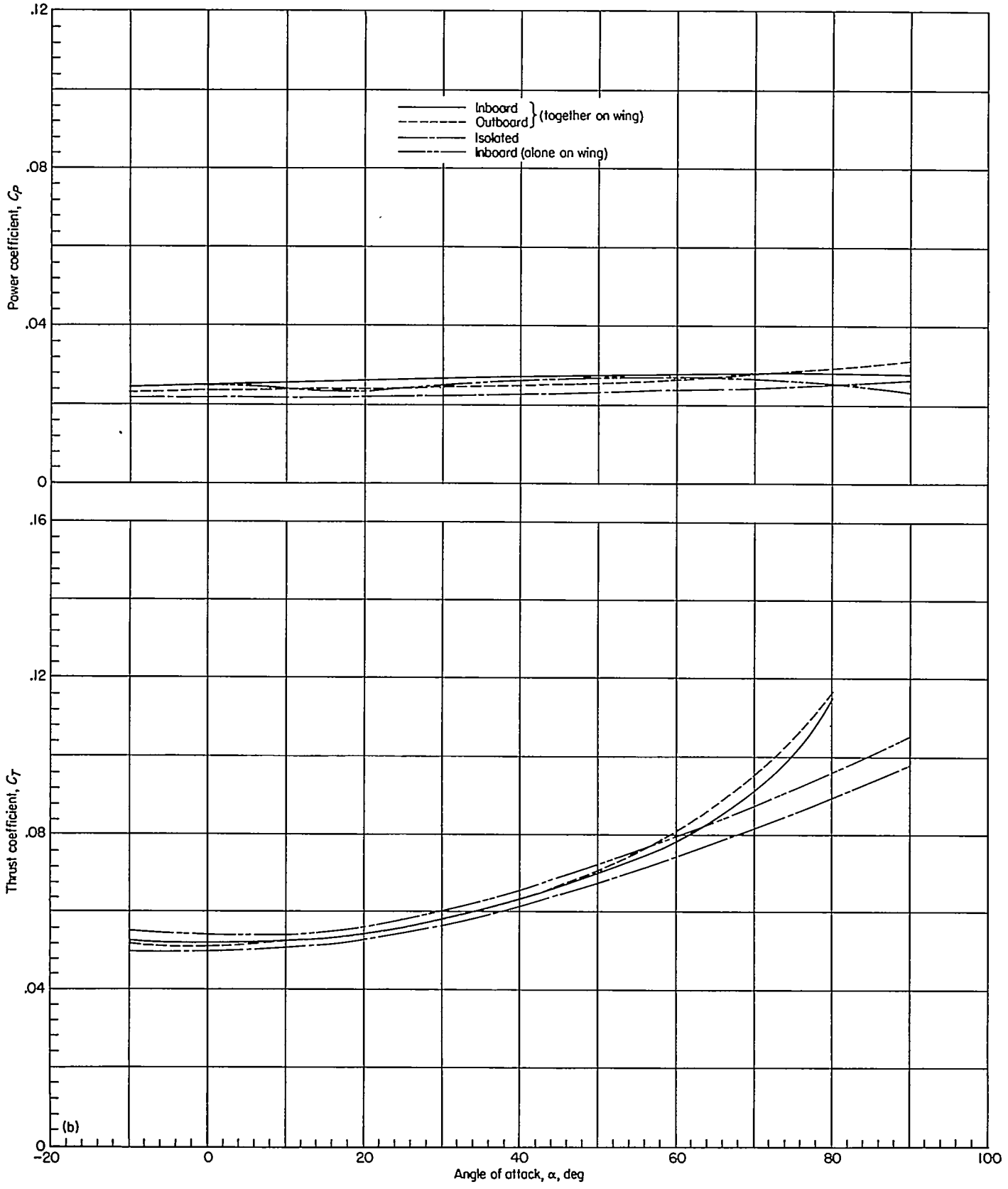

(b) $T_c''=0.71$; $\beta_{0.75R}=8°$.

FIGURE 9.—Continued.

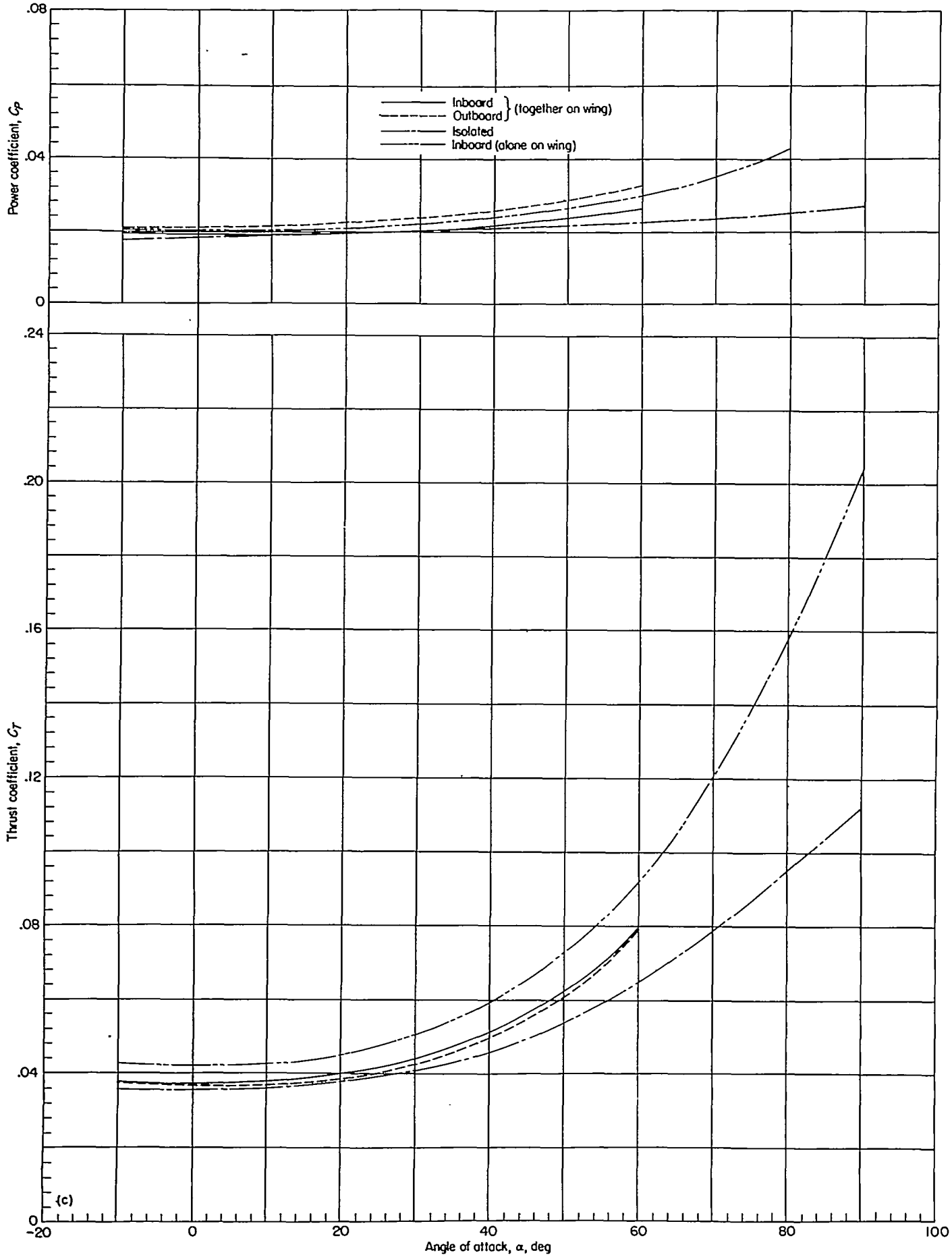

(c) $T_c''=0.50$; $\beta_{0.75R}=8°$.

FIGURE 9.—Continued.

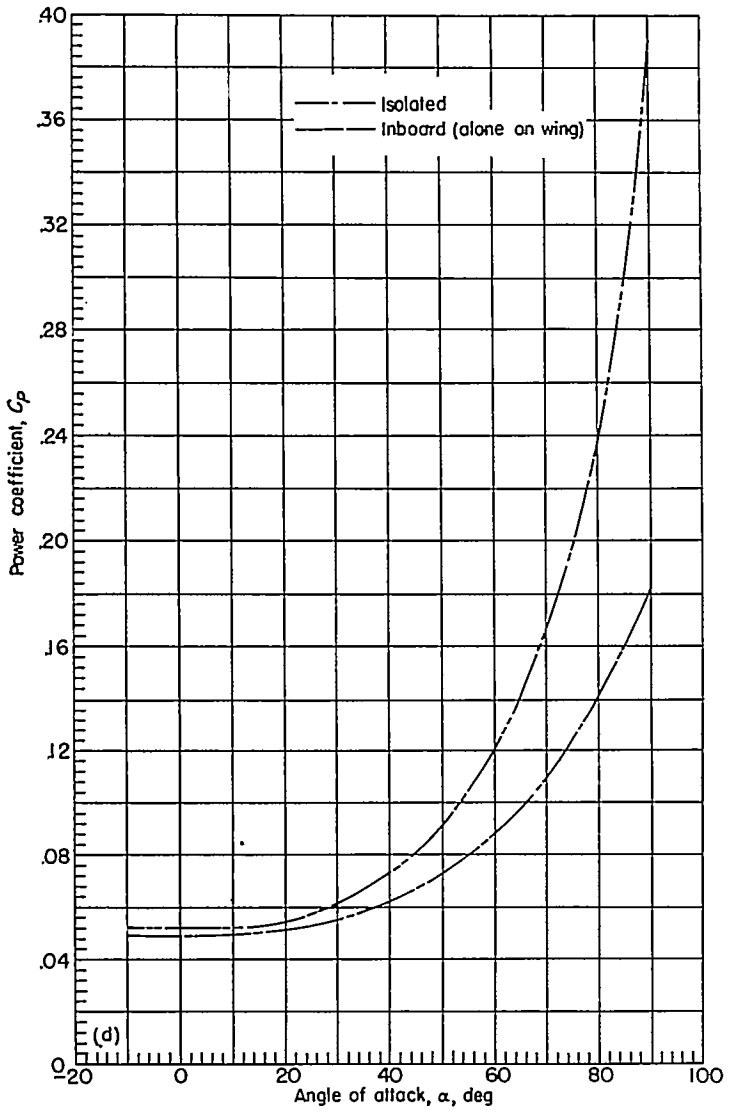

(d) $T_c''=0.20$; $\beta_{0.75R}=20°$.

FIGURE 9.—Continued.

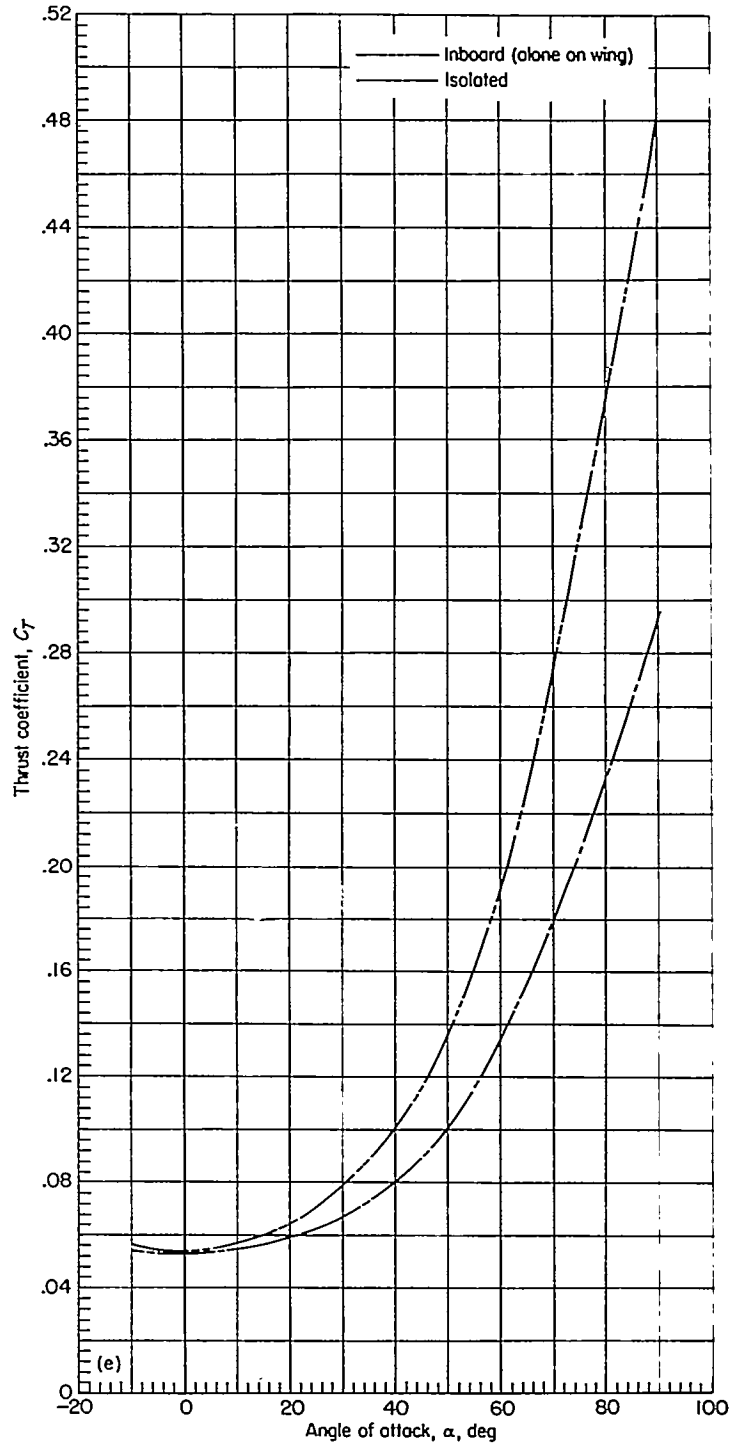

(e) $T_c''=0.20$; $\beta_{0.75R}=20°$.

FIGURE 9.—Concluded.

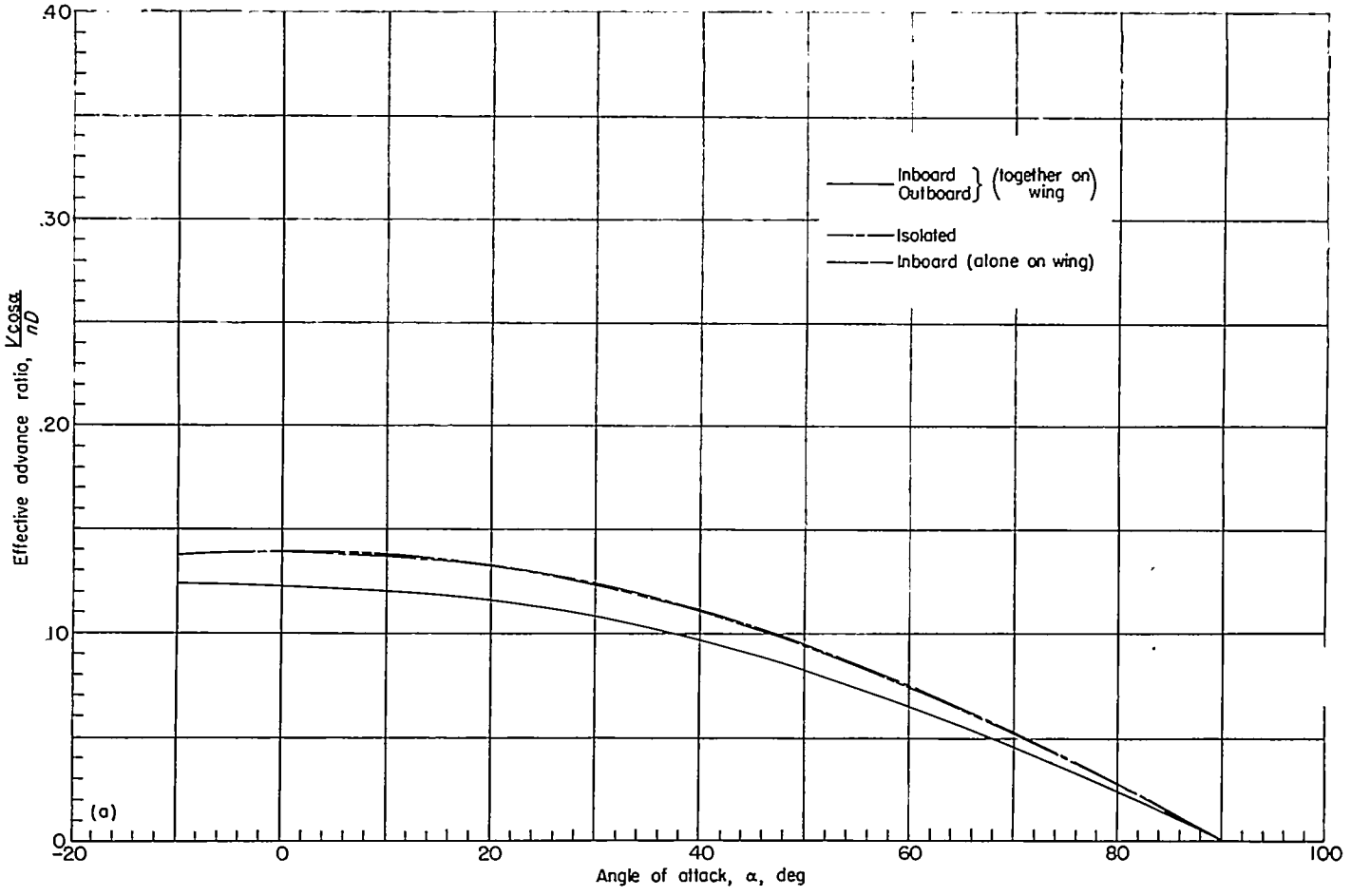

(a) $T_c''=0.91$; $\beta_{0.75R}=8°$.

FIGURE 10.—Comparison of advance ratios for various configurations at constant thrust through angle-of-attack range.

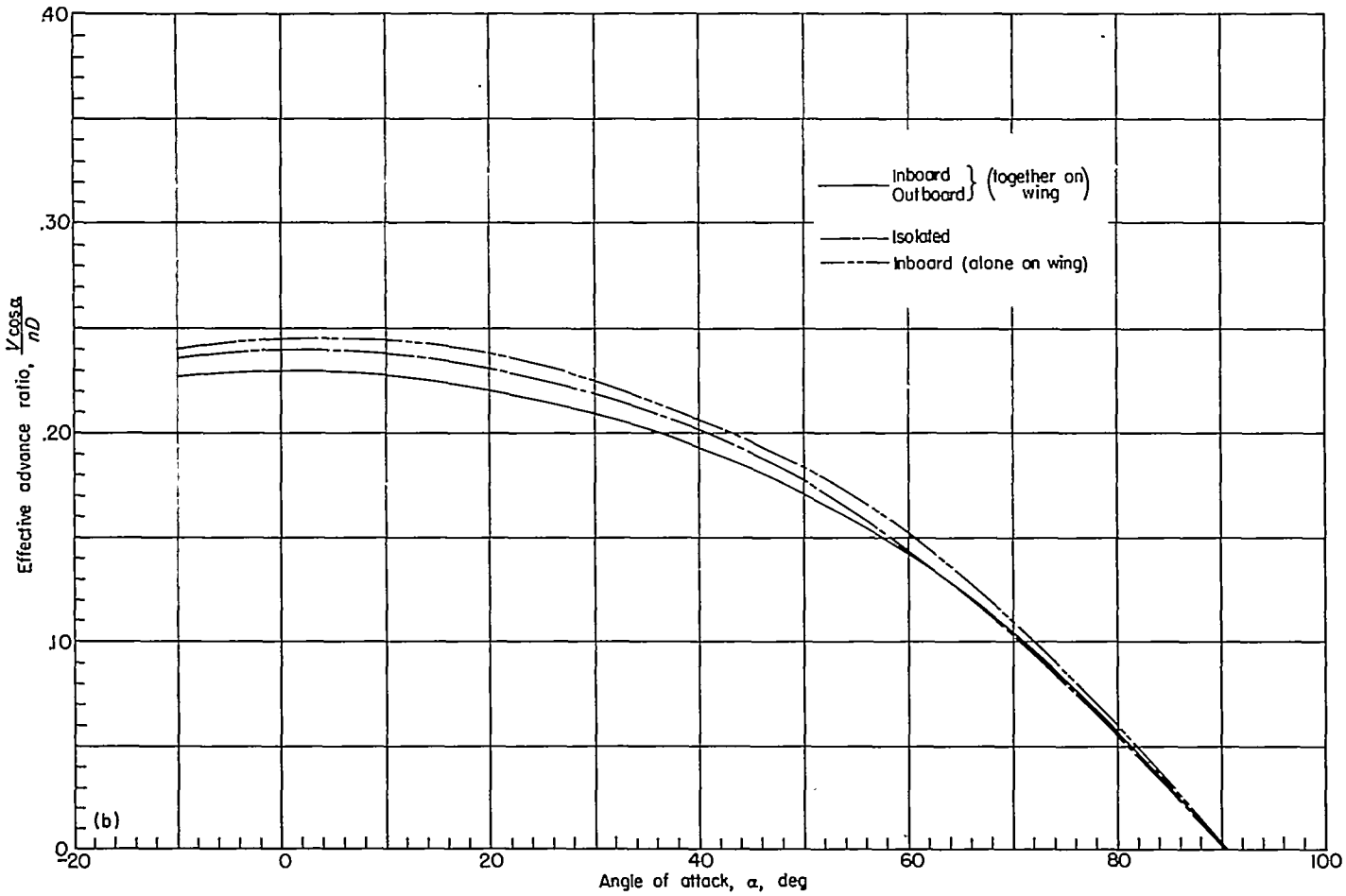

(b) $T_c''=0.71$; $\beta_{0.75R}=8°$.

FIGURE 10.—Continued.

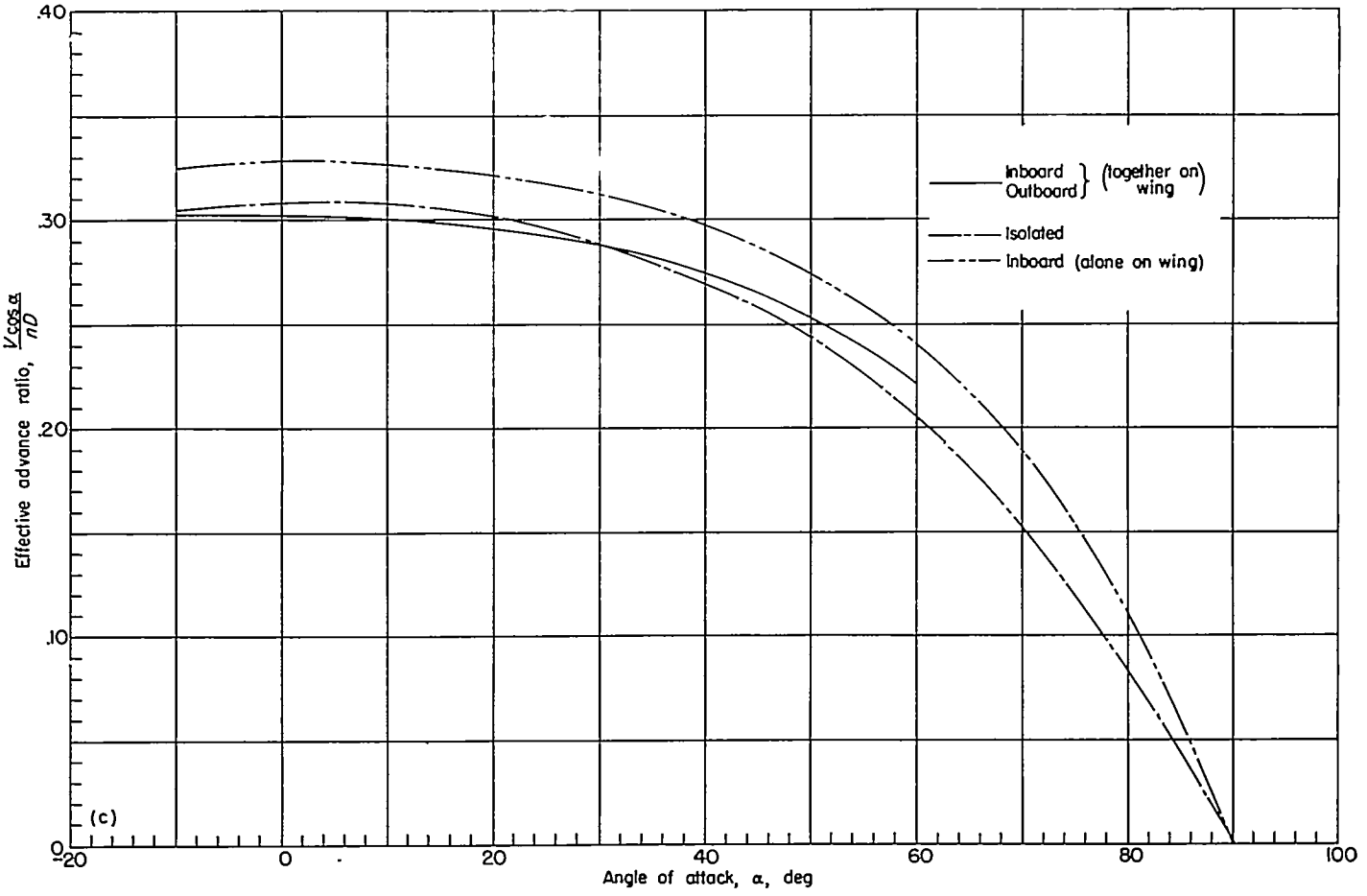

(c) $T_c''=0.50$; $\beta_{0.75R}=8°$.

FIGURE 10.—Continued.

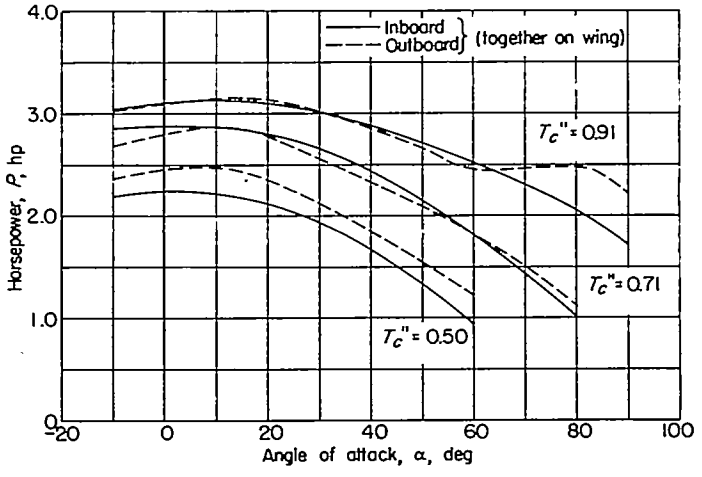

FIGURE 11.—Variation of horsepower required for constant thrust through angle-of-attack range. $\beta_{0.75R}=8°$.

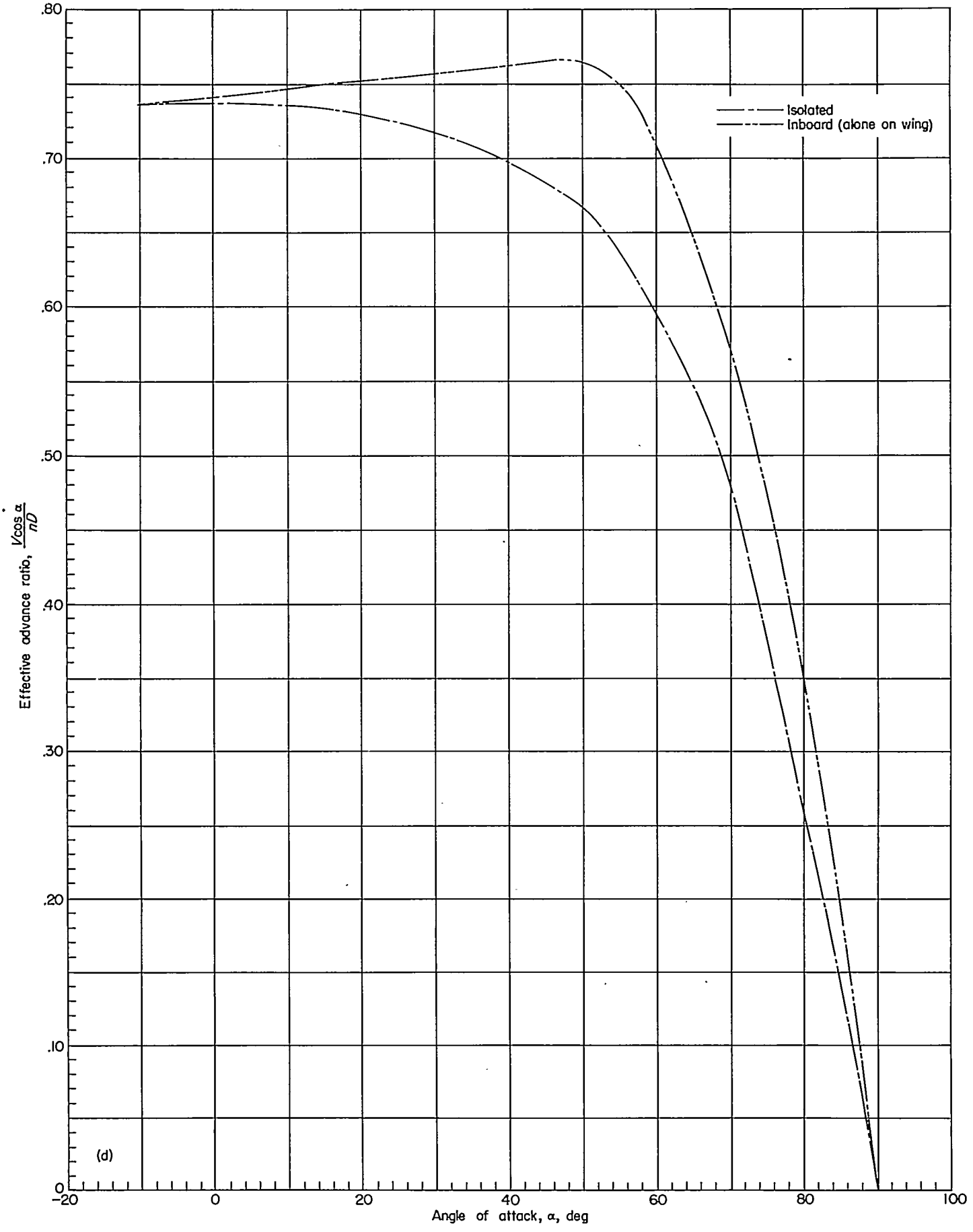

(d) $T_c''=0.20$; $\beta_{0.75R}=20°$.

FIGURE 10.—Concluded.

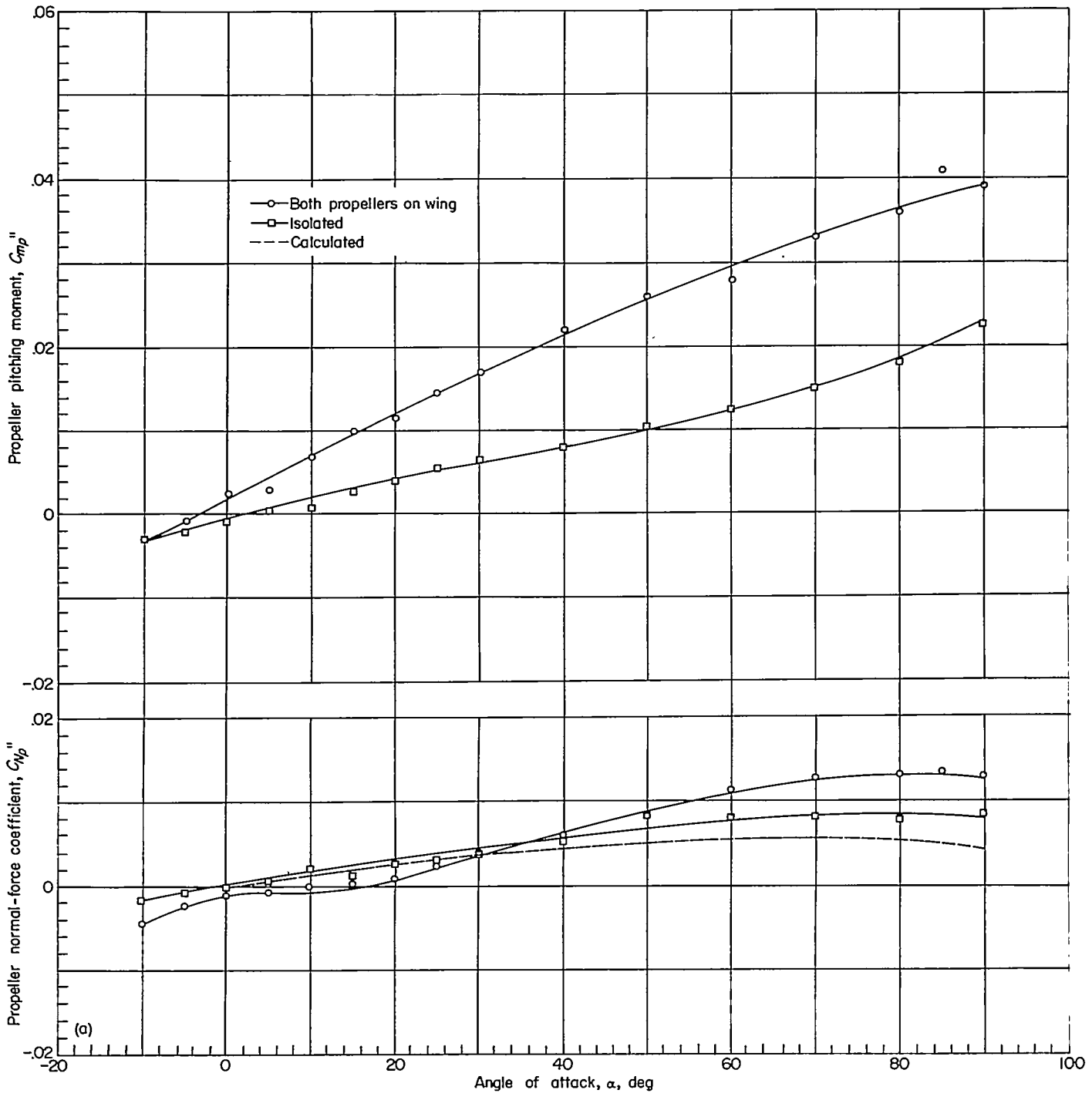

(a) $T_c''=0.91$.

FIGURE 12.—Variation of direct pitching-moment and normal-force coefficients of the outboard propeller through angle-of-attack range.

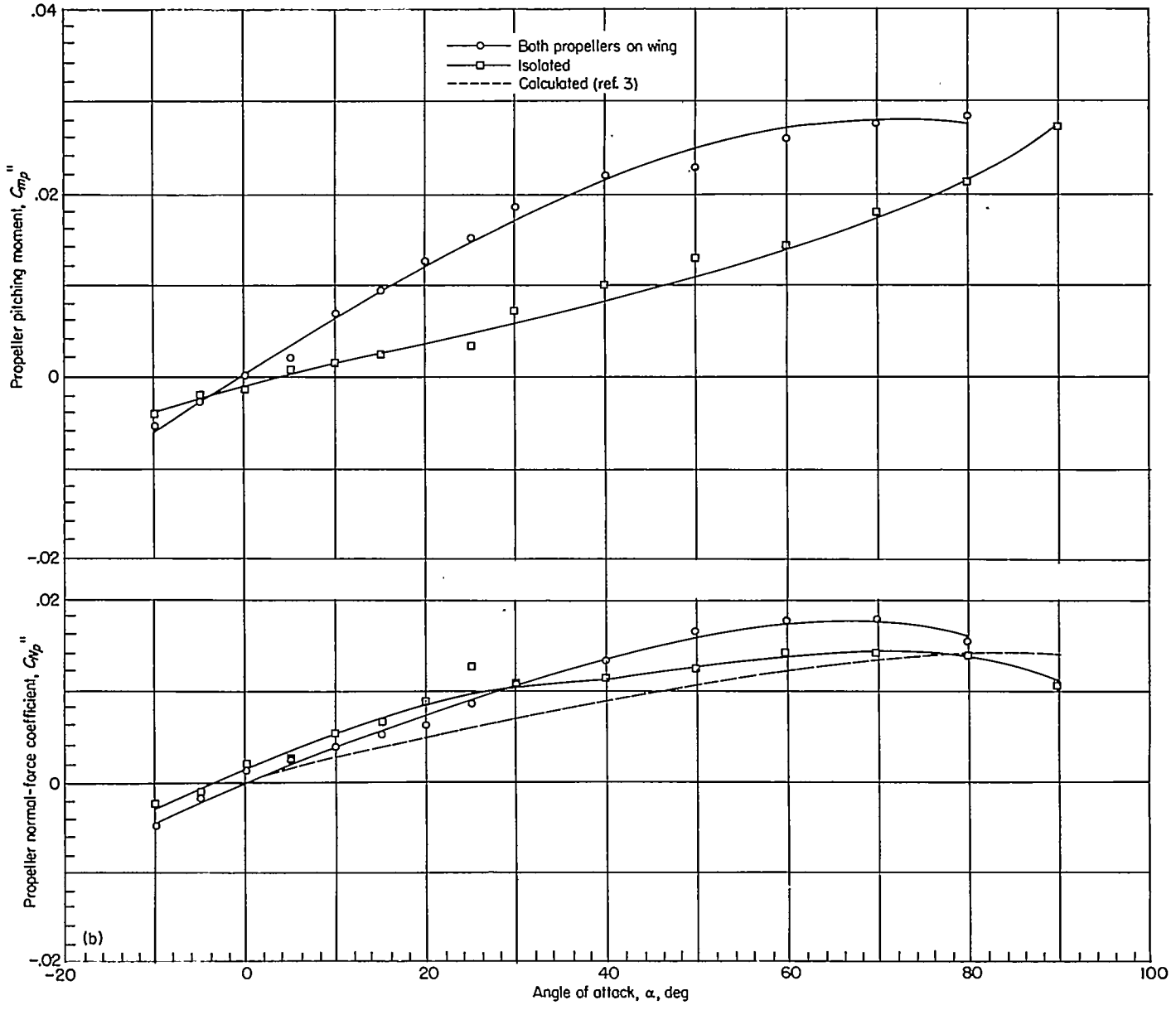

(b) $T_c''=0.71$.

FIGURE 12.—Continued.

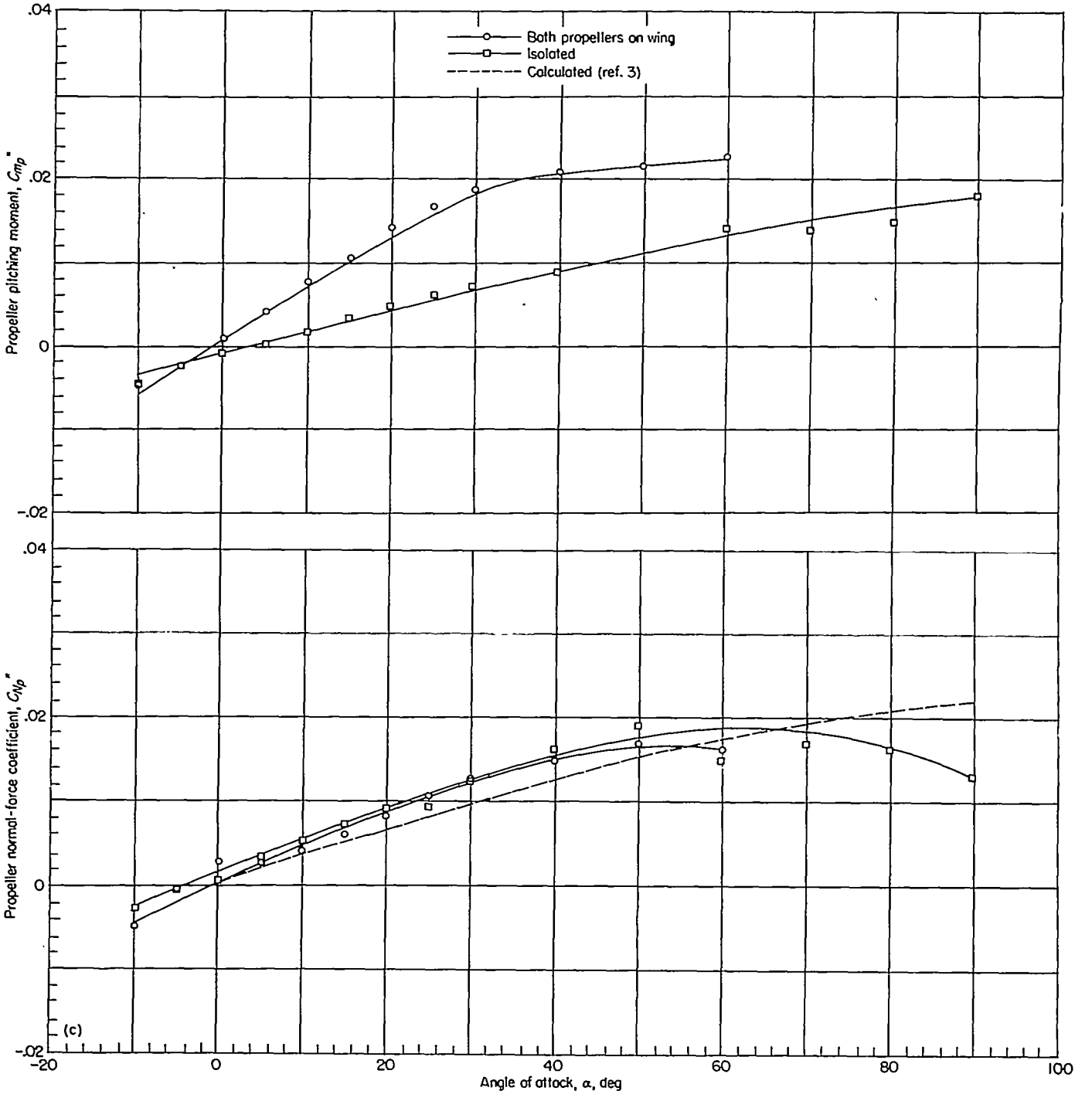

(c) $T_c''=0.50$.

FIGURE 12.—Concluded.

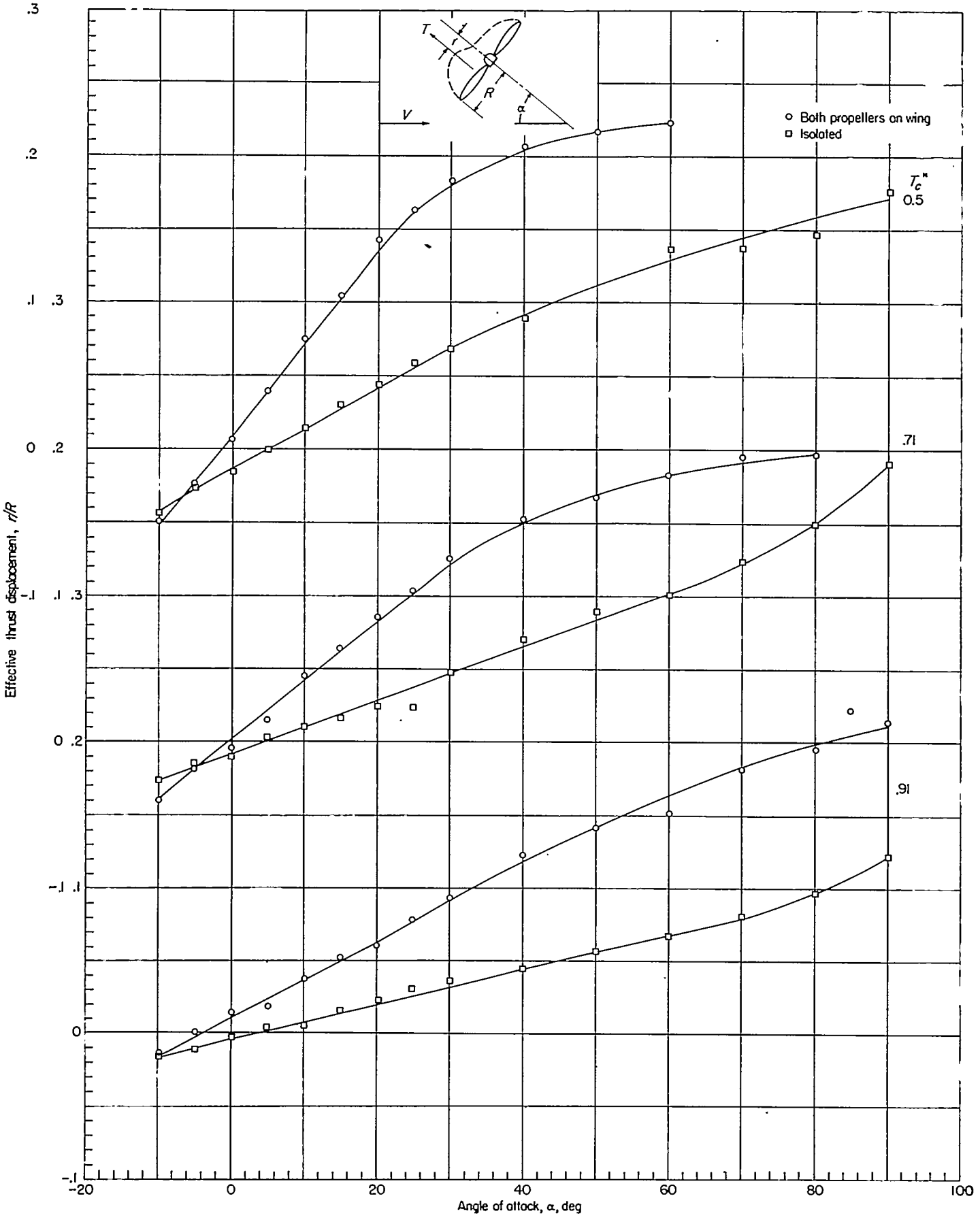

FIGURE 13.—Effect of angle of attack on effective thrust displacement from thrust axis as determined by $\frac{r}{R}=\frac{C_{m_p}''S\bar{c}}{T_c''\frac{\pi}{8}D^3}$ for outboard propeller.

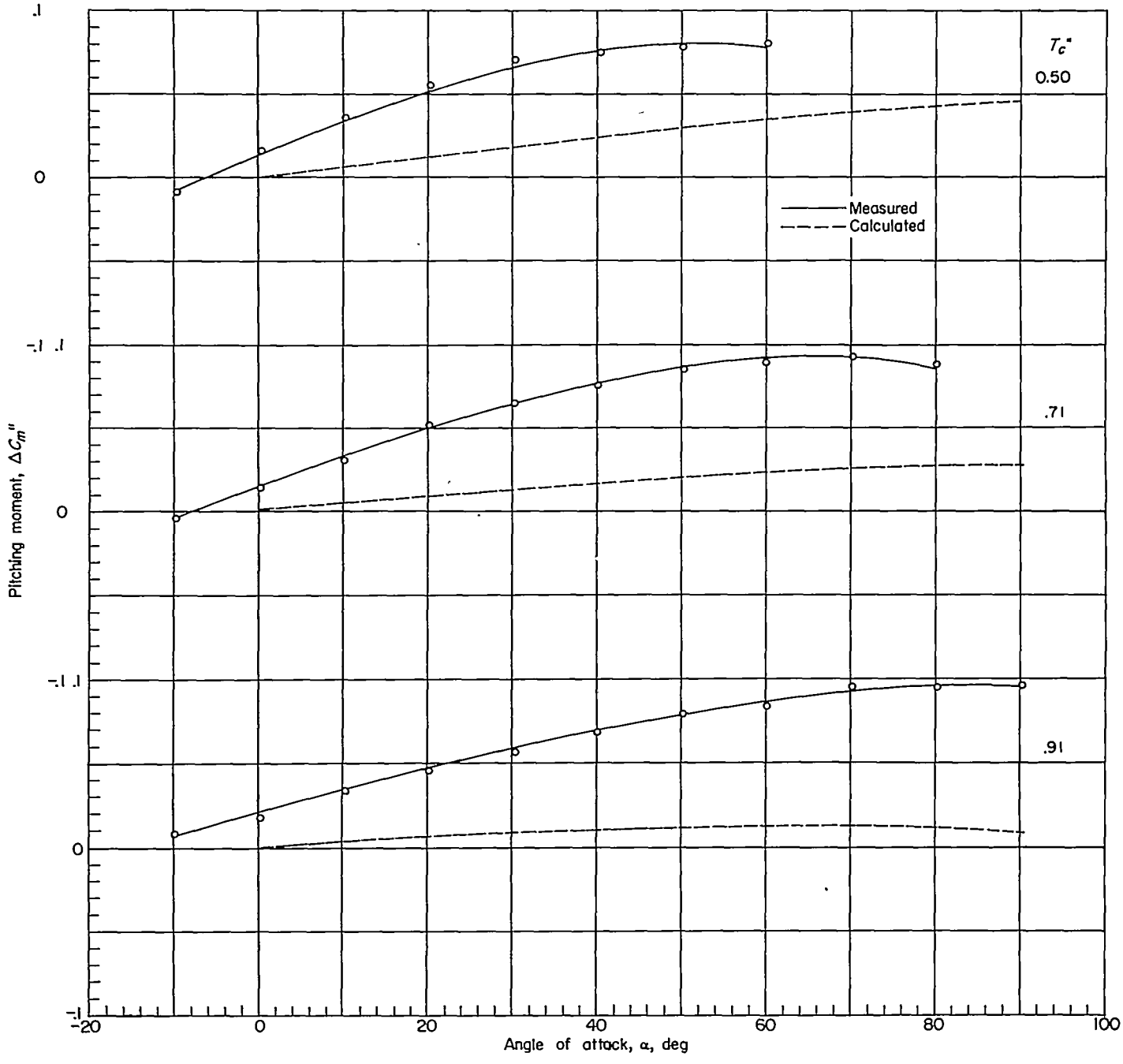

FIGURE 14.—Increment of model pitching moment due to the propellers (two propellers in operation).

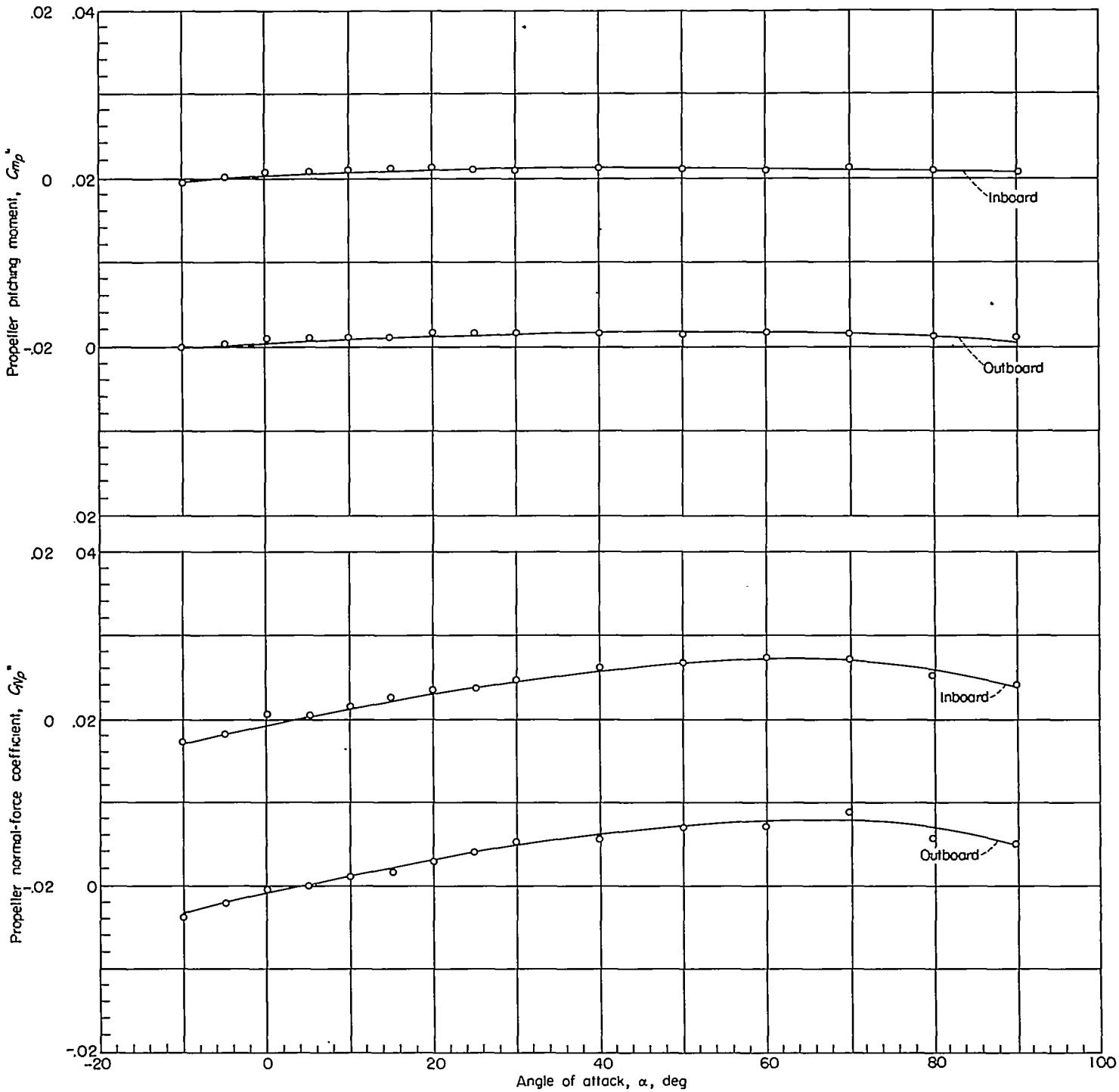

FIGURE 15.—Variation of the spinner characteristics with angle of attack. Propeller blades removed; spinner not rotating.

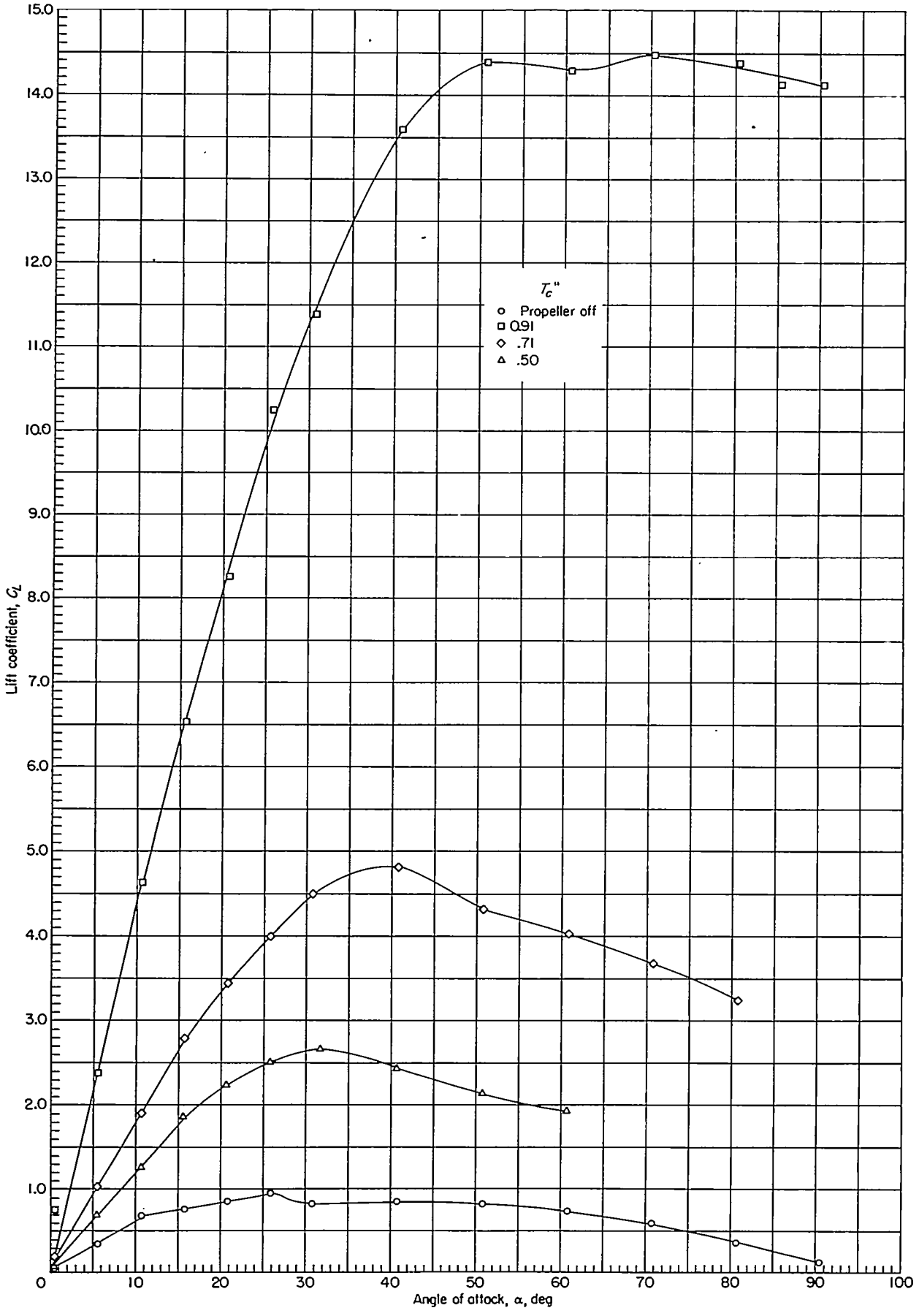

FIGURE 16.—Lift characteristics of model with various thrust coefficients. Lift coefficient based on free-stream dynamic pressure.

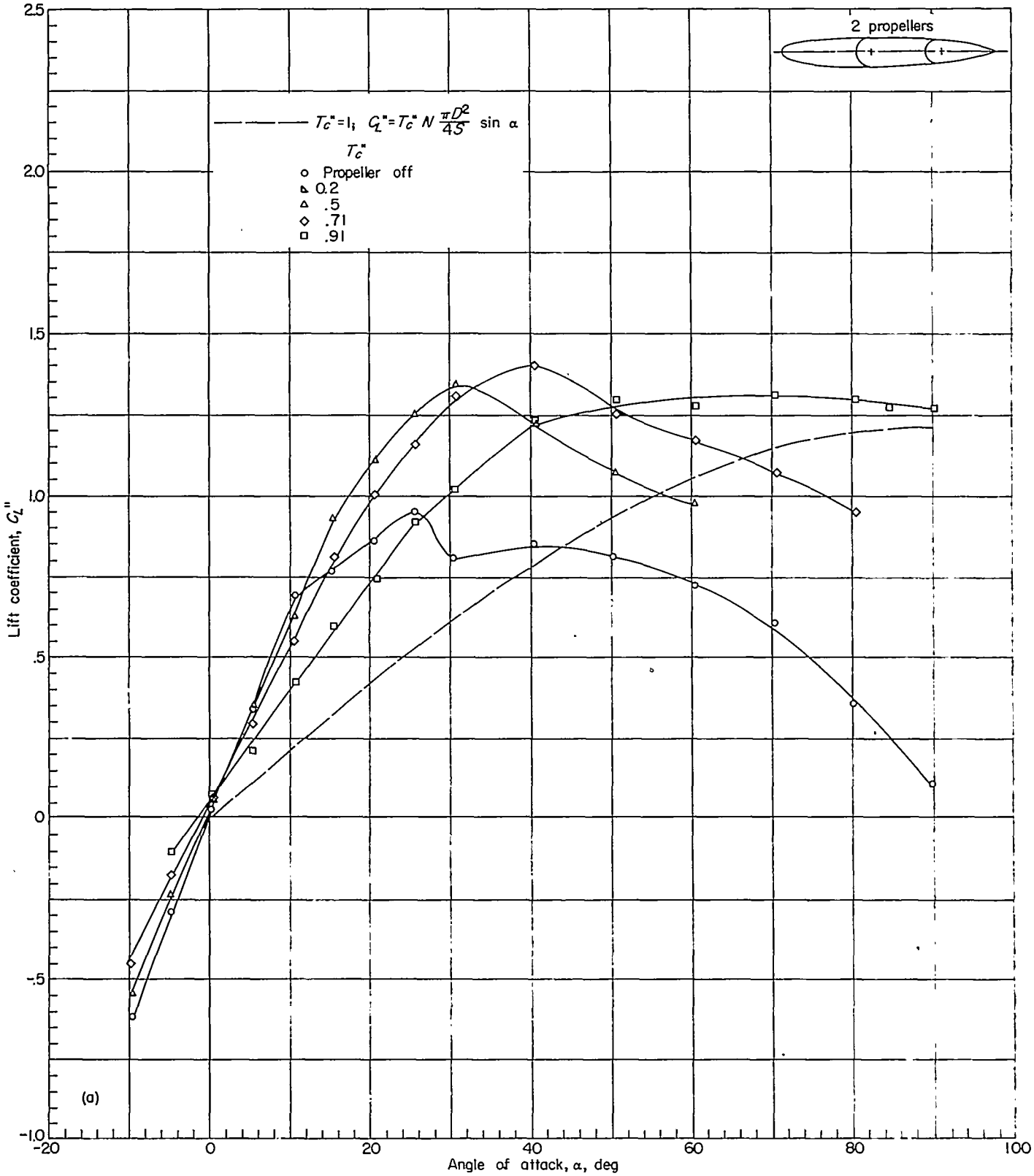

(a) Lift coefficient.

FIGURE 17.—Effect of thrust coefficient on aerodynamic characteristics of model with two propellers operating.

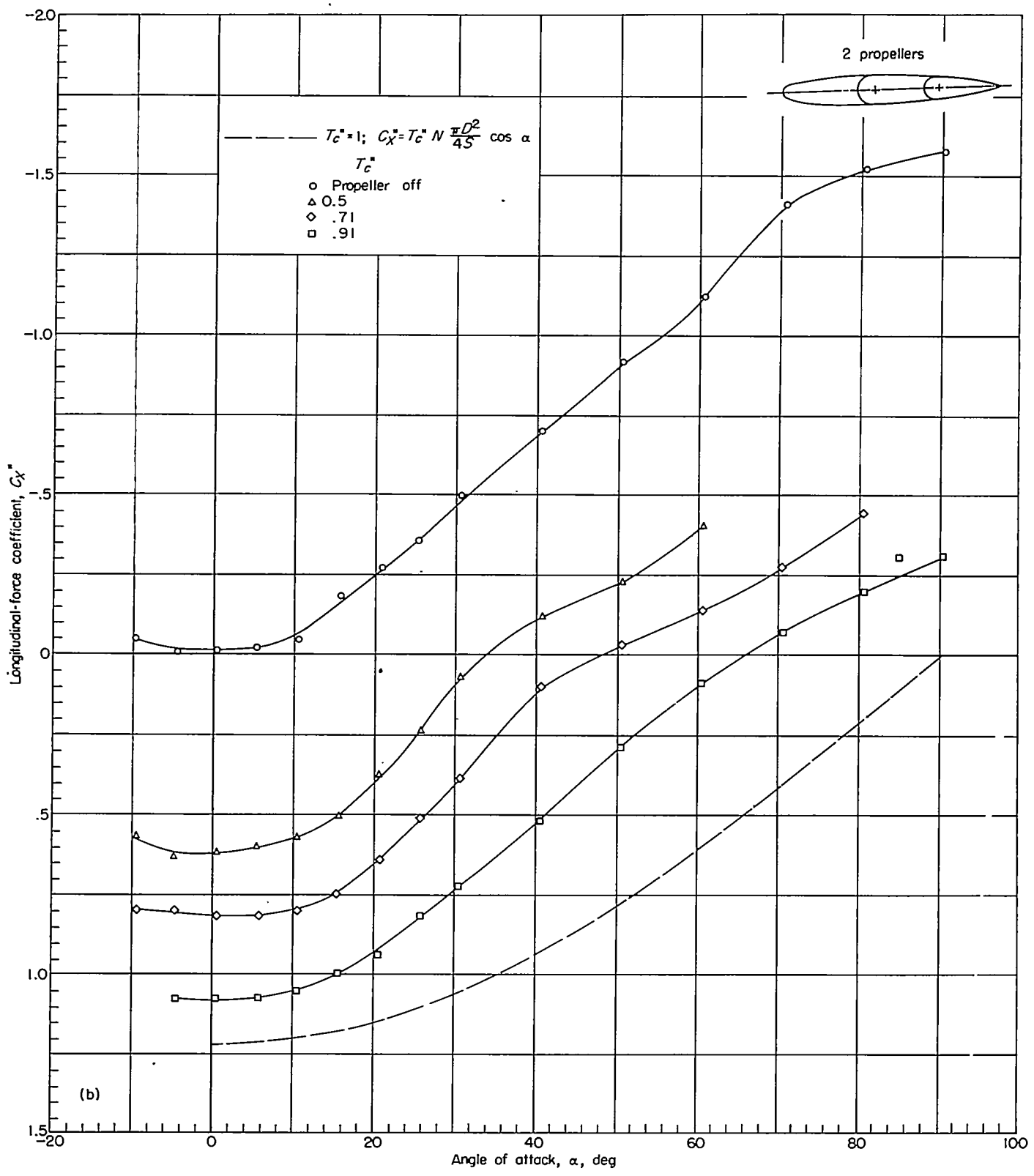

(b) Longitudinal-force coefficient.

FIGURE 17.—Continued.

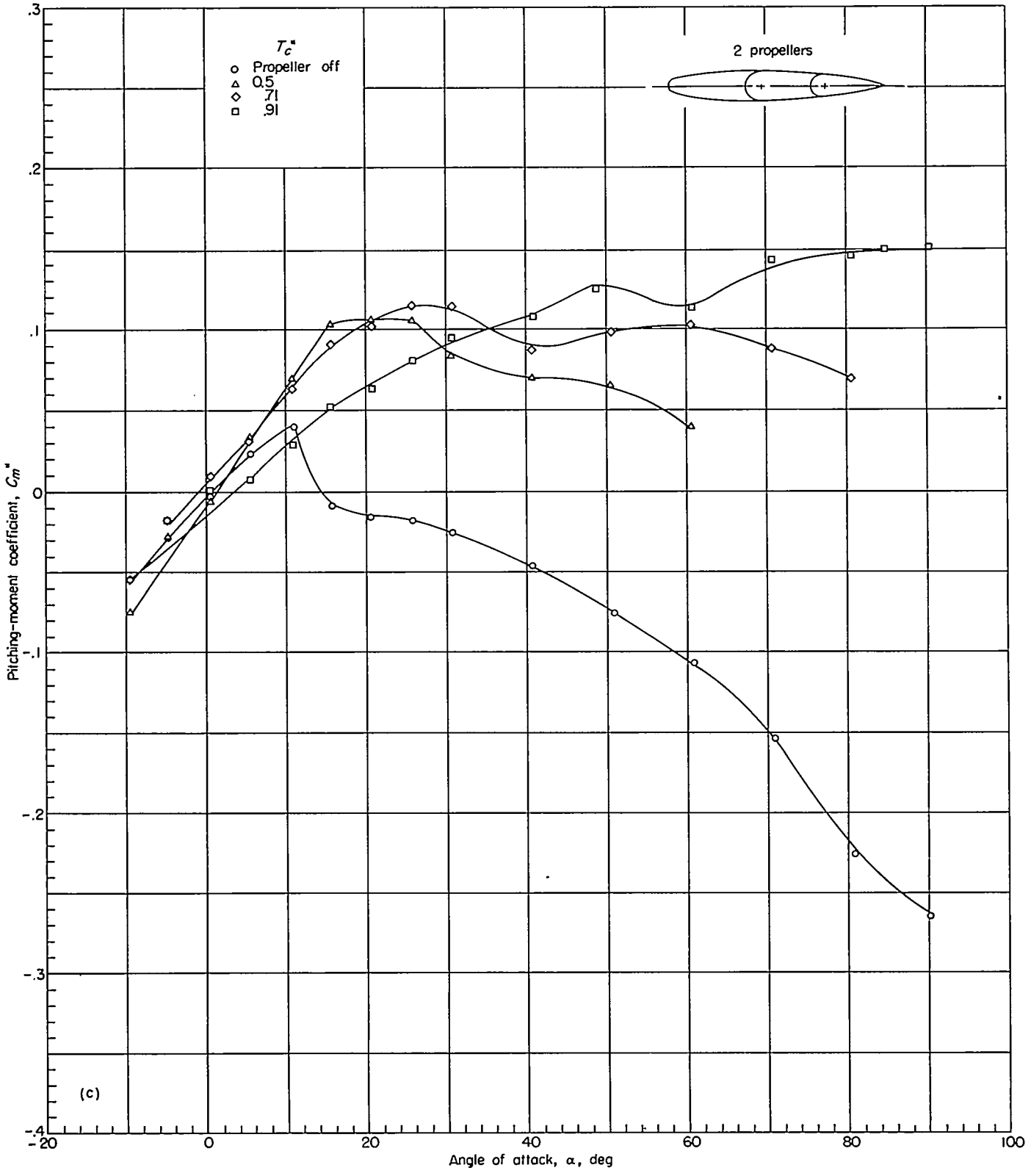

(c) Pitching-moment coefficient.

FIGURE 17.—Concluded.

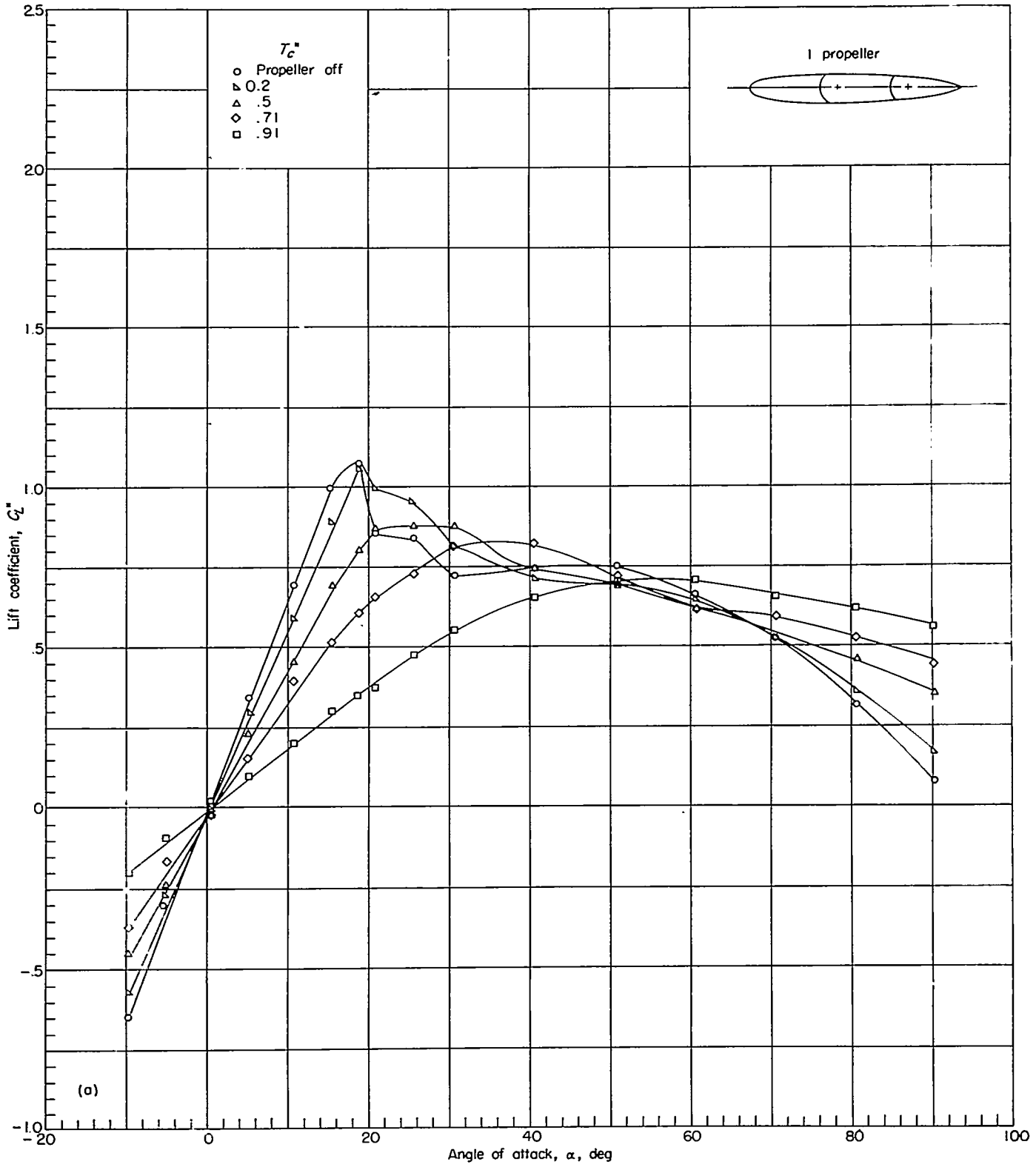

(a) Lift coefficient.

FIGURE 18.—Effect of thrust coefficient on aerodynamic characteristics of model with inboard propeller only.

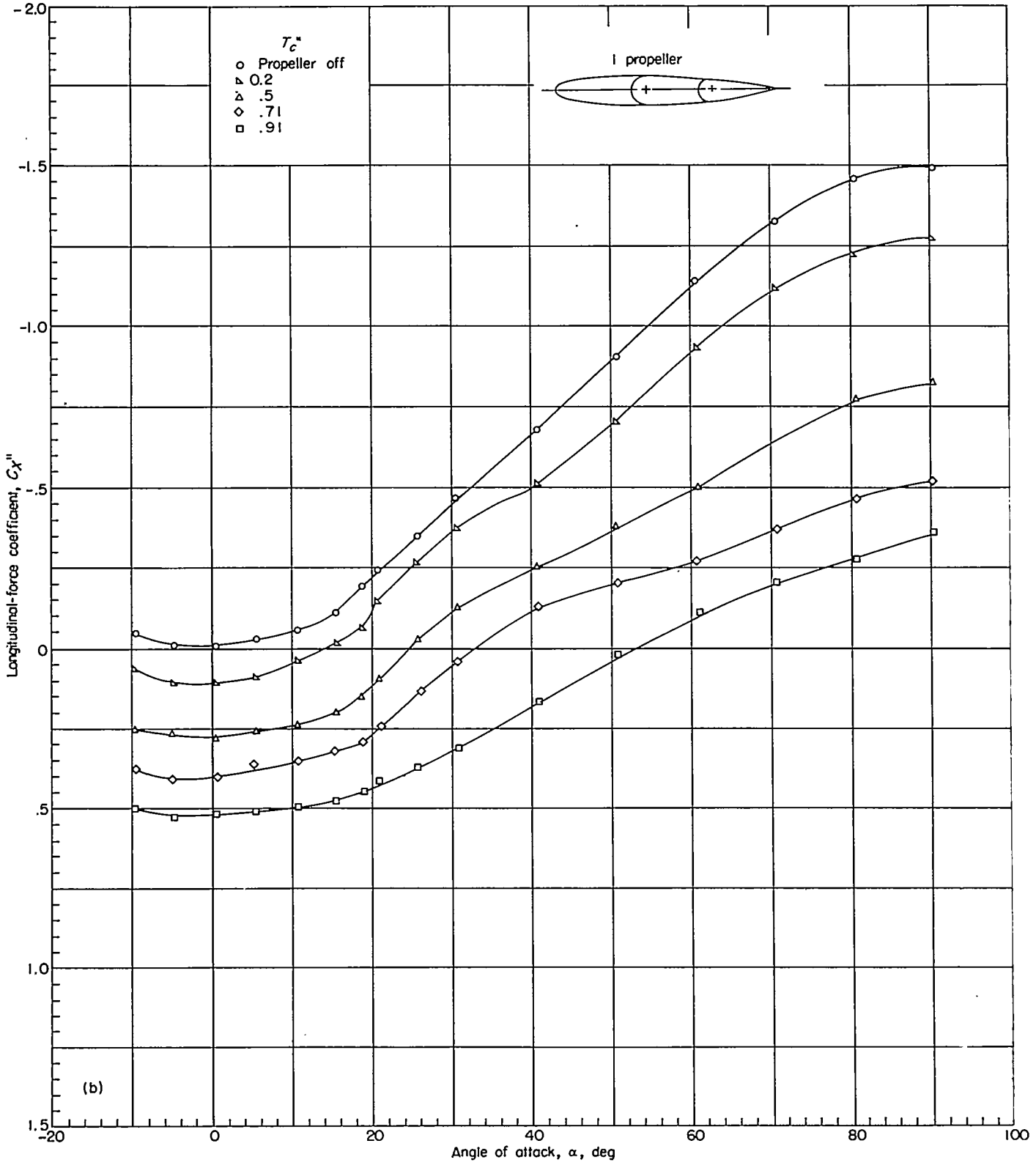

(b) Longitudinal-force coefficient.

FIGURE 18.—Continued.

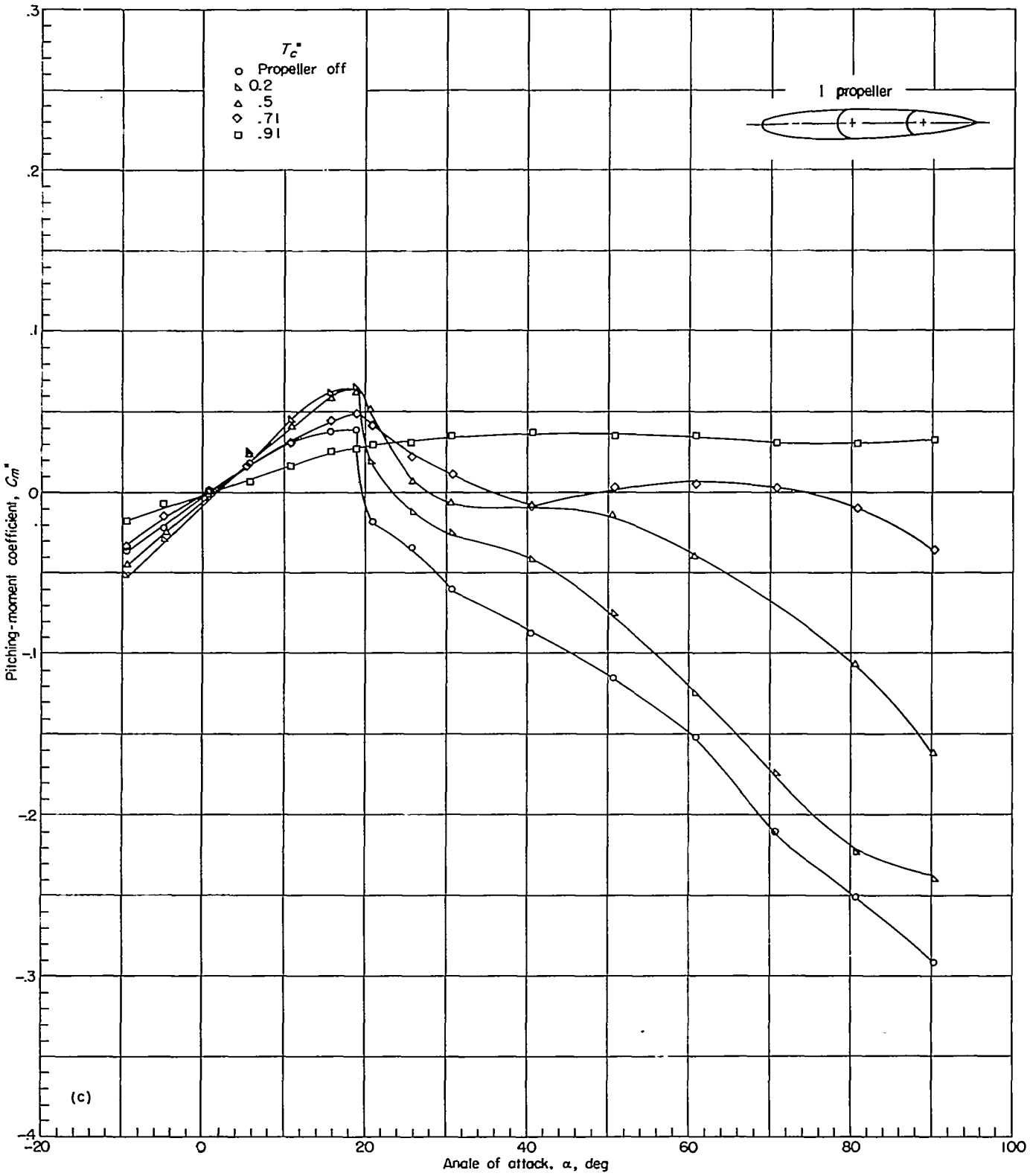

(c) Pitching-moment coefficient.

FIGURE 18.—Concluded.

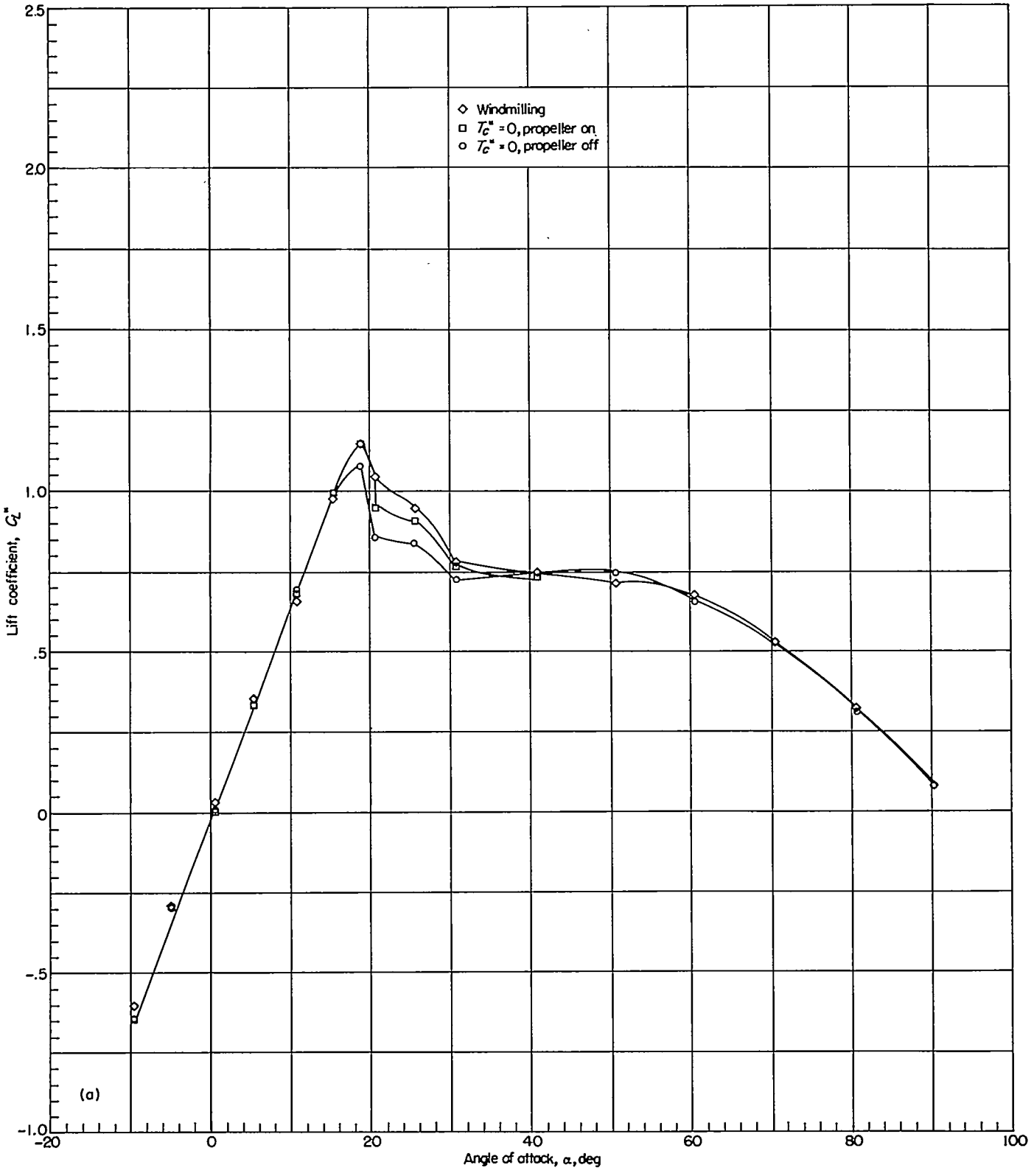

(a) Lift coefficient.

FIGURE 19.—Effect of propeller on aerodynamic characteristics of the model. Propeller windmilling, propeller at $T_c''=0$, and propeller-removed conditions.

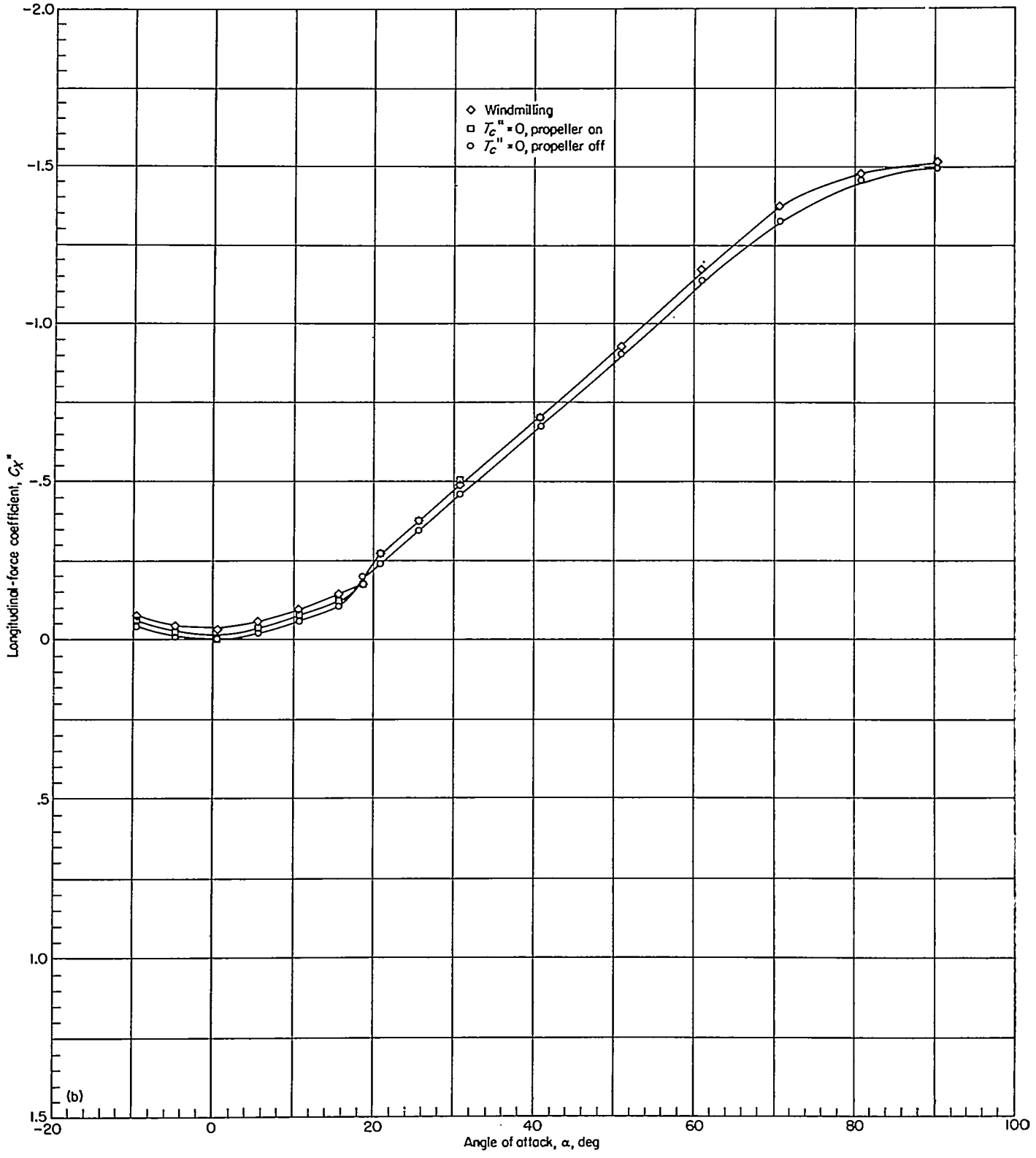

(b) Longitudinal-force coefficient.

FIGURE 19.—Continued.

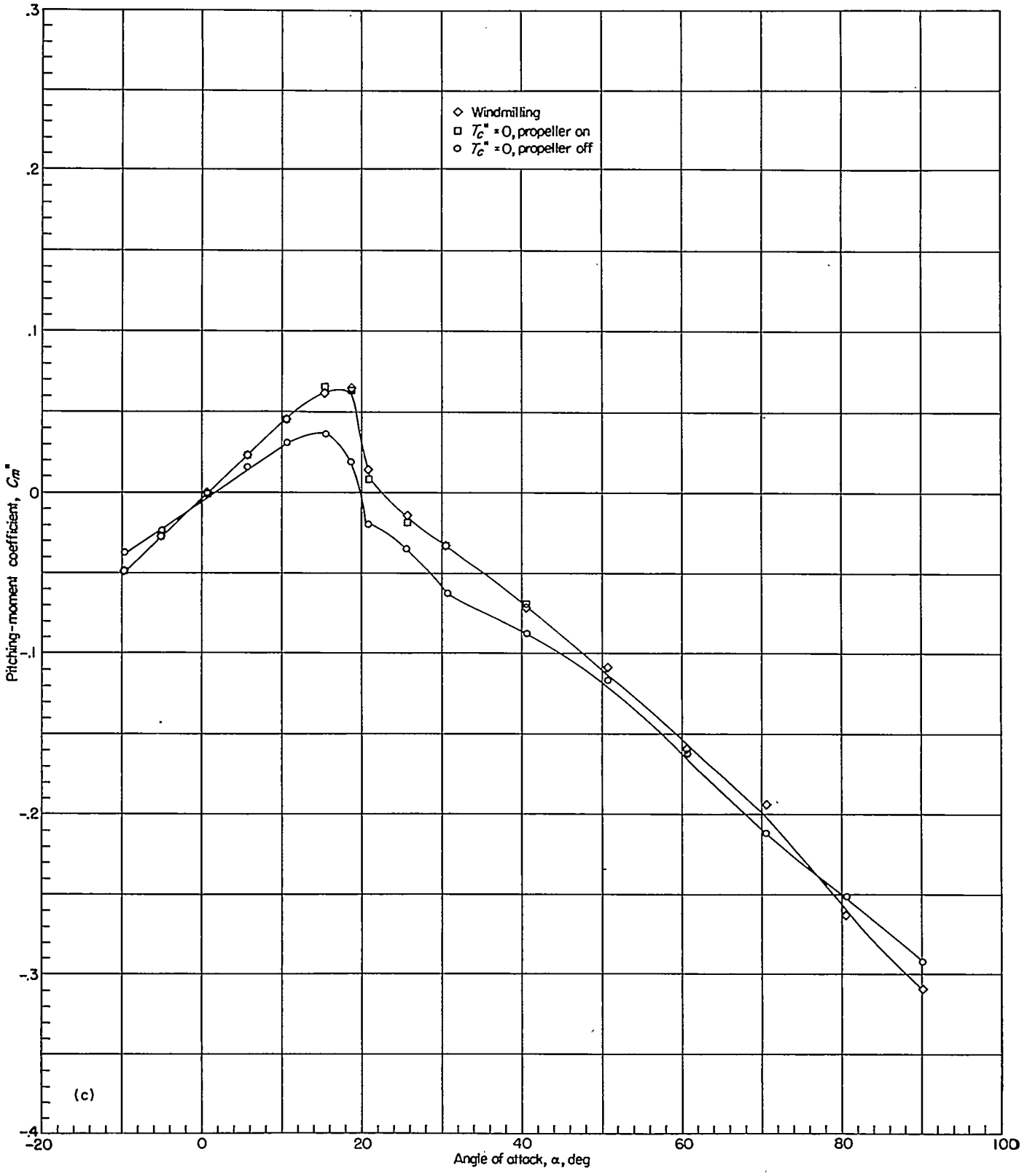

(c) Pitching-moment coefficient.

FIGURE 19.—Concluded.

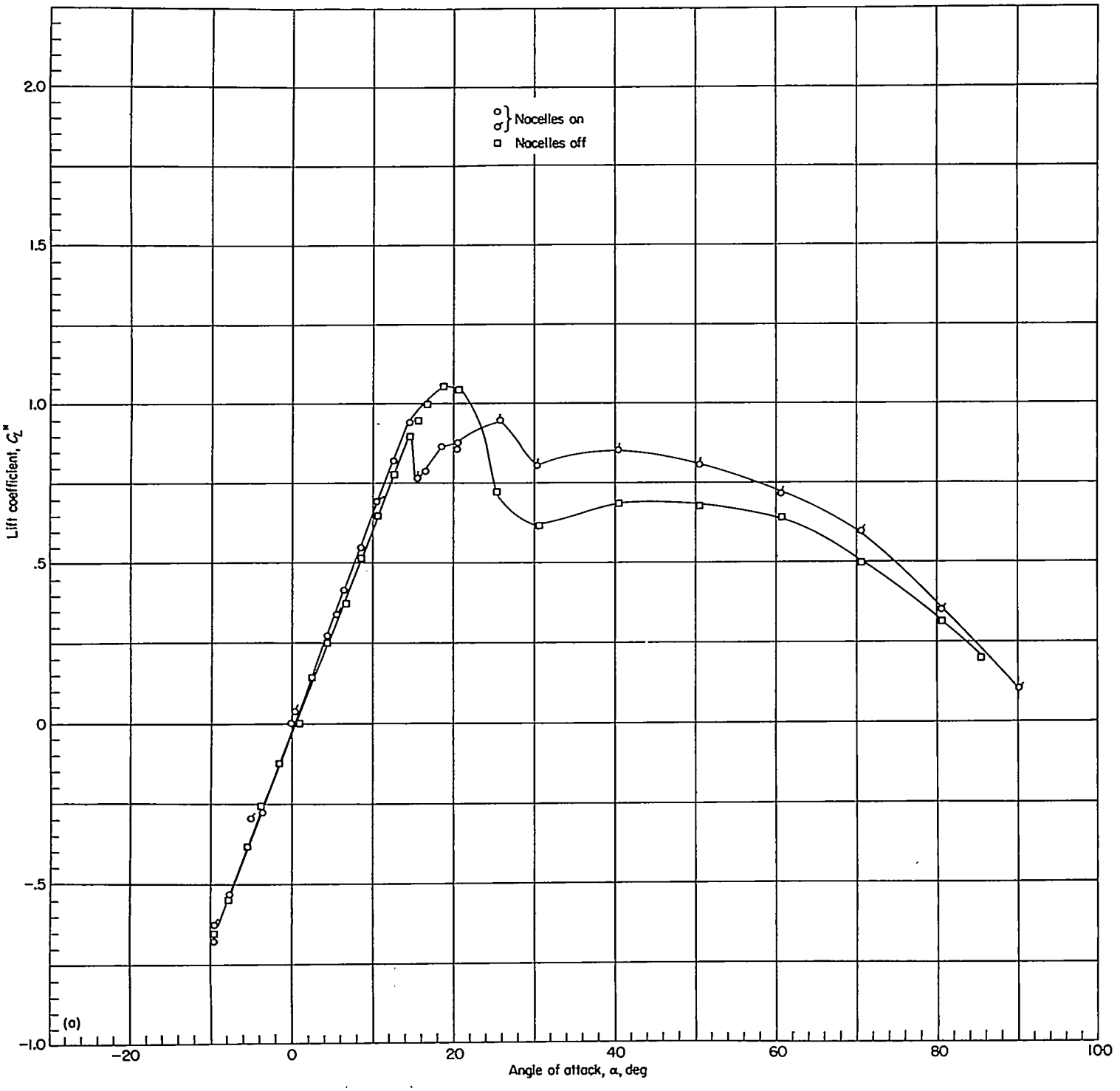

(a) Lift coefficient.

FIGURE 20.—Effect of nacelles on aerodynamic characteristics of the model with propellers off. (Flagged symbols indicate check tests.)

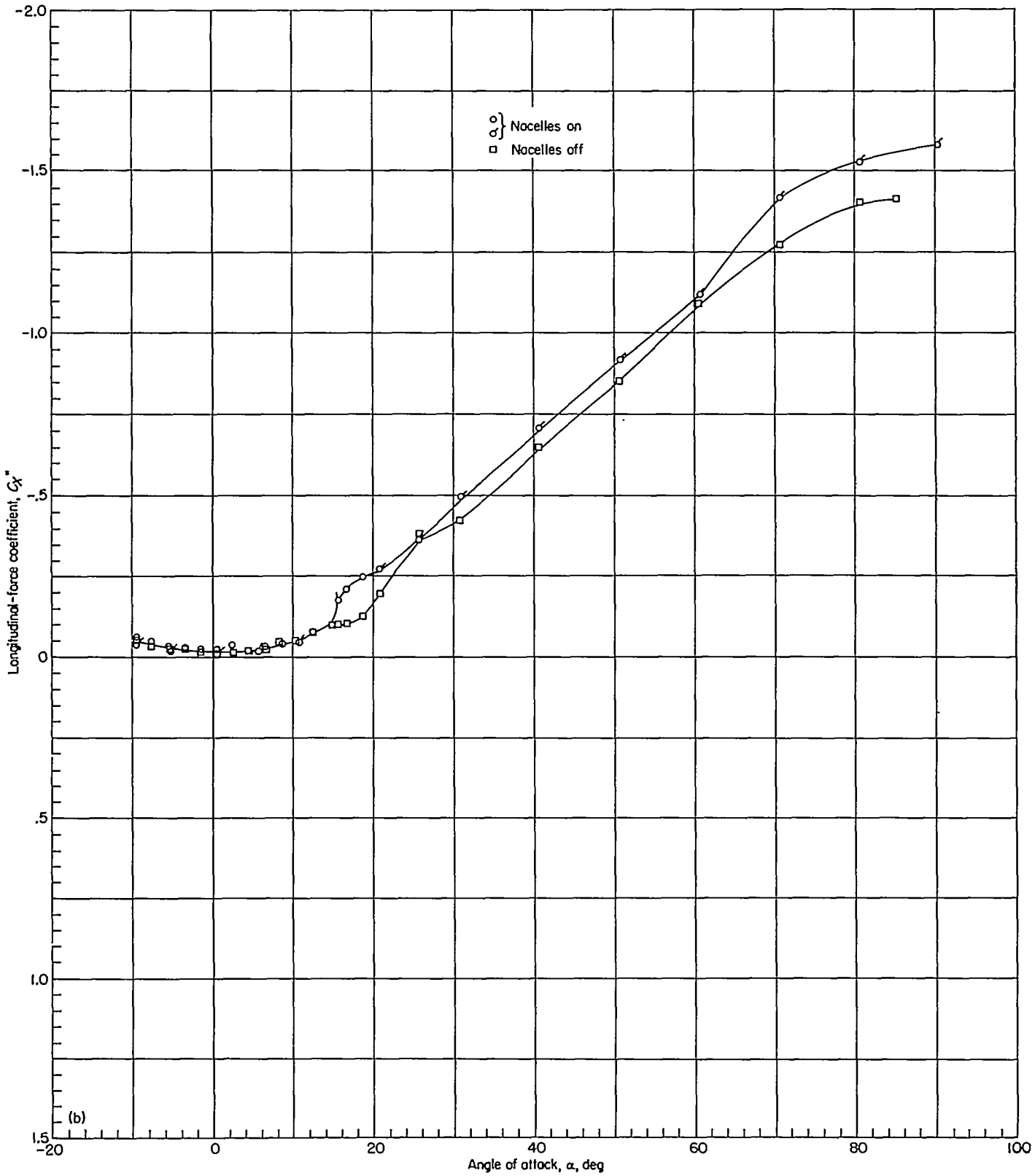

(b) Longitudinal-force coefficient.

FIGURE 20.—Continued.

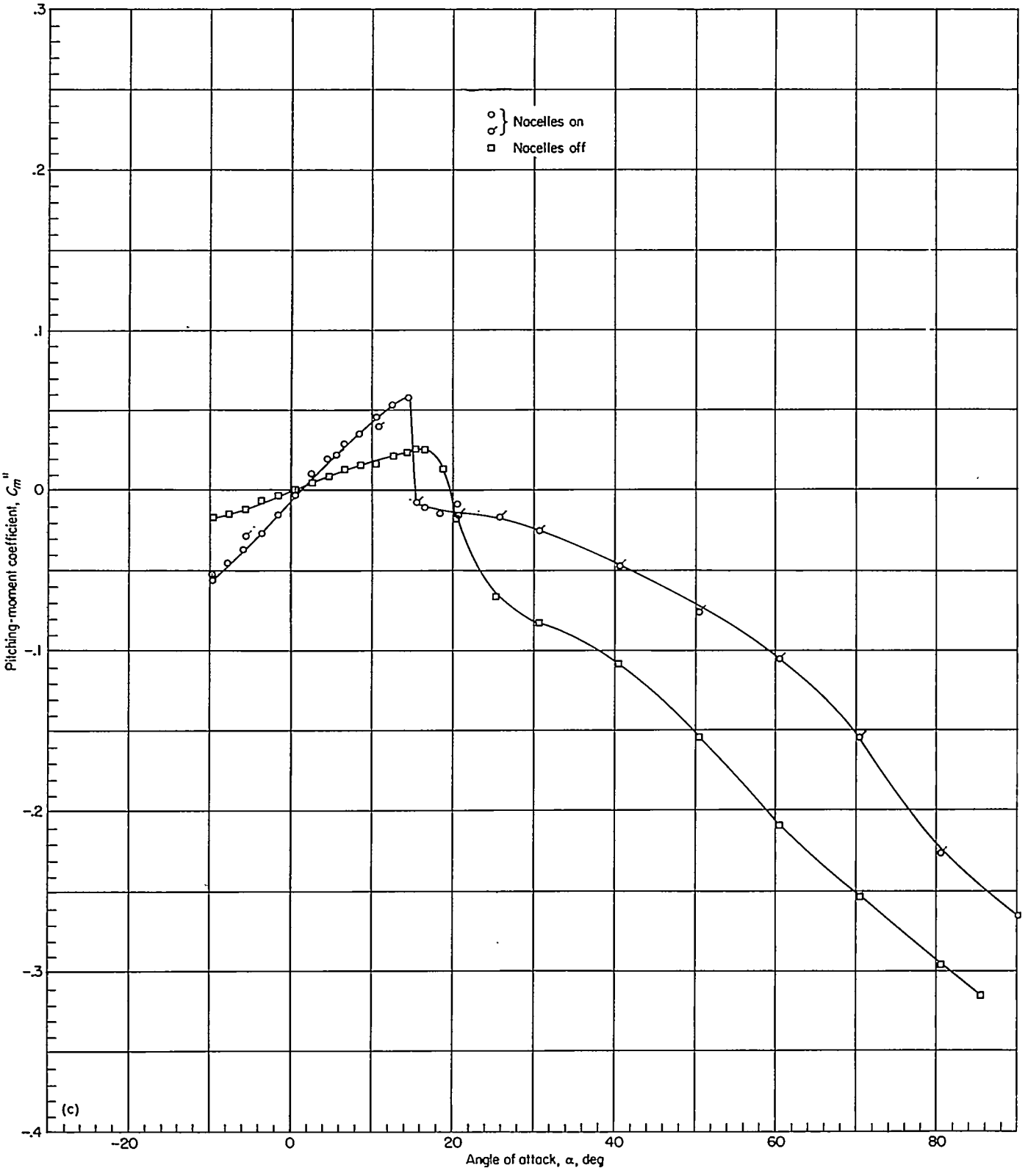

(c) Pitching-moment coefficient.

FIGURE 20.—Concluded.

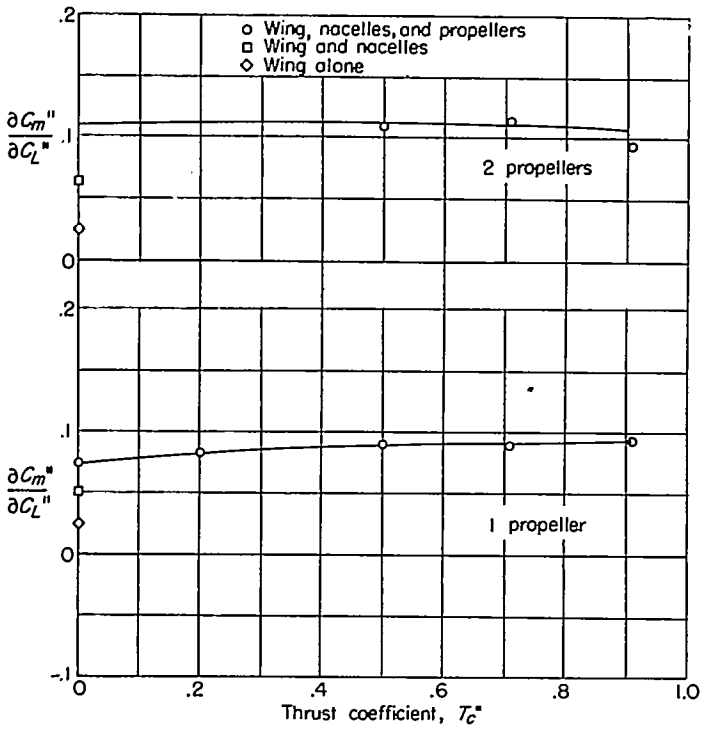

FIGURE 21.—Variation with thrust coefficient of longitudinal-stability parameter $\partial C_m''/\partial C_L''$ near $\alpha=0°$.

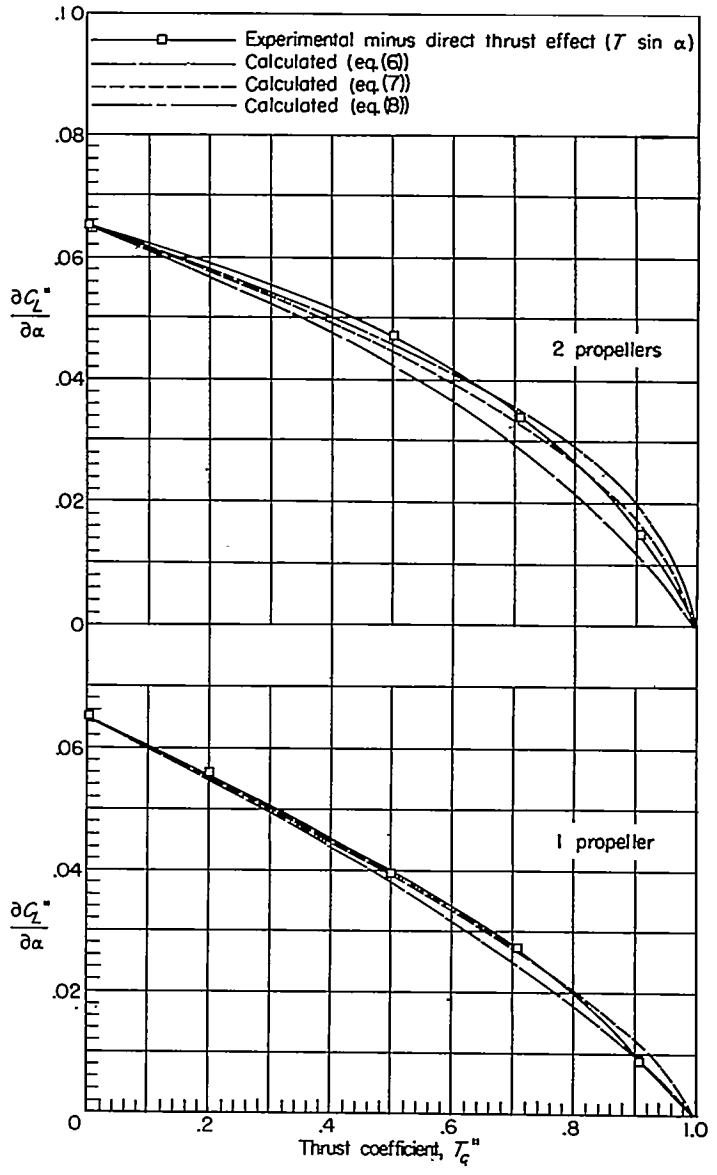

FIGURE 22.—Variation of $\partial C_L''/\partial \alpha$ with thrust coefficient near $\alpha=0°$.

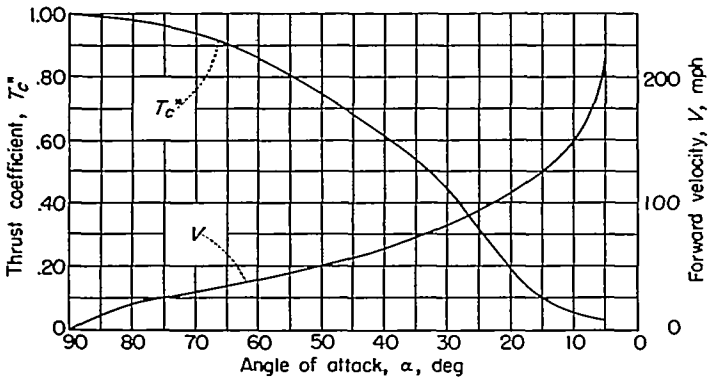

FIGURE 23.—Variation with angle of attack of thrust coefficient required and velocity attained in level flight by assumed airplane. $W/S=40$ pounds per square foot.

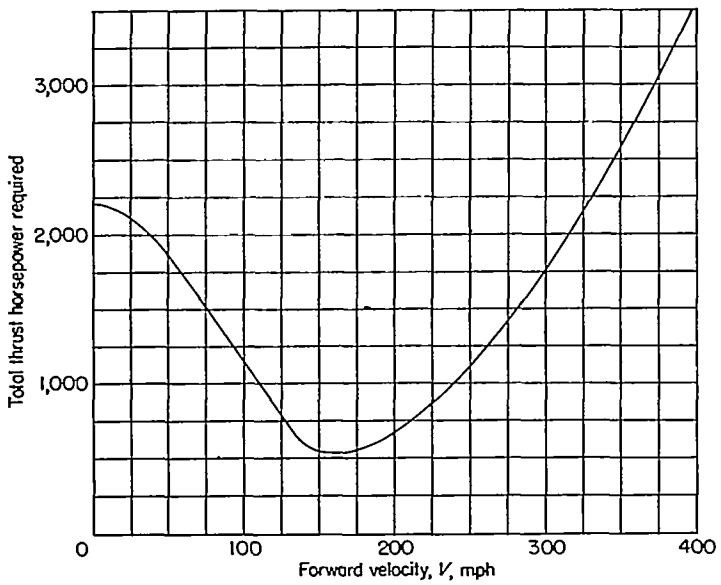

FIGURE 24.—Variation of thrust horsepower required for level flight for assumed airplane.

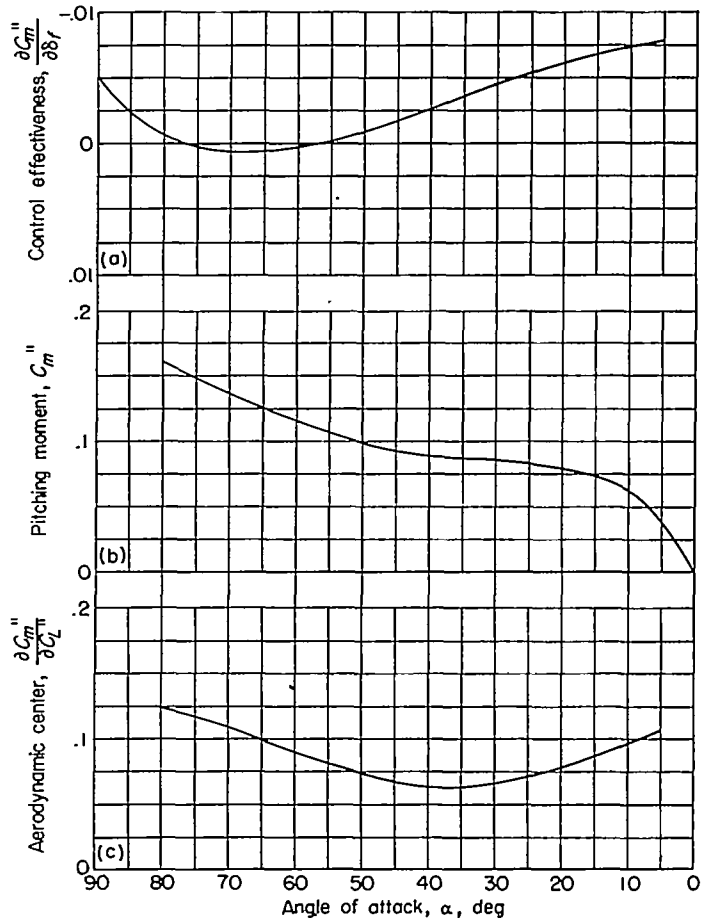

(a) 30%c full-span-flap effectiveness.
(b) Untrimmed pitching moment.
(c) Aerodynamic-center location.

FIGURE 25.—Pitching characteristics of assumed airplane through angle-of-attack range.